Chapter 8
Theory and Application of Transient Infinite Elements for Simulating Contaminant Transport Problems in Fractured Porous Media of Infinite Domains

Numerical simulation of contaminant transport in fractured porous media of infinite domains is a complex problem in various aspects. The solution for this kind of problem becomes more difficult once practical considerations, such as the infinite extension of the problem domain, the leakage effect between the porous medium and the fissured network, the characterization of the fissured network and other physical and chemical parameters, are appropriately included in the analysis (Rowe and Booker 1989, 1990a, 1991). On the other hand, the practical problems involving contaminant transport in fractured porous media have received rapidly increasing attention as a result of the treatment of industrial and agricultural wastes, the evaluation of potential contamination from nuclear power plants and the disposal activities of wastes from our daily lives. For the purpose of a better understanding of contaminant transport processes, it is imperative to develop an efficient and effective numerical method for simulating transient contaminant (i.e. mass in a general term) transport problems in fractured porous media of infinite domains.

Since a naturally fractured system contains various discontinuities, most of the immobile pore-fluid resides in low permeability, disjoint matrix blocks, while most of the mobile pore-fluid resides in the high permeability, interconnected fissured network. When contaminant transport takes place in such a system, both advection and dispersion are dominant processes within the fissured network, while dispersion may be a dominant process in the porous matrix. Generally, advection is due to the bulk movement of pore-fluid, which is caused by a pore-fluid pressure gradient, according to Darcy's law (Phillips 1991; Nield and Bejan 1992; Zhao et al. 1997, 1998, 1999a). Dispersion is due to the irregular movement of pore-fluid in a porous medium (Bear 1972; Bear and Bachmat 1990). On the microscopic scale (i.e. the pore scale), these irregularities are caused by the tortuosity of flow paths, while on the macroscopic scale, they are caused by the presence of zones of different permeabilities. To simulate a naturally fractured system appropriately, the double porosity model (Barenblatt et al. 1960; Duguid and Lee 1977; Valliappan and Naghadah 1990) may be the best choice because it bridges the gap between equivalent porous media and discrete fracture theory. For the double porosity model, the porous block and fissured network are viewed as two overlapping continua. Equations of mass

C. Zhao, *Dynamic and Transient Infinite Elements*, Advances in Geophysical and Environmental Mechanics and Mathematics, DOI 10.1007/978-3-642-00846-7_8,

transport for each continuum can be linked by a leakage term that describes the mass exchange between the two overlapping continua.

In terms of modelling an infinite medium, the coupled computational method of finite elements and infinite elements (Bettess 1977, 1980, 1992; Chow and Smith 1981; Medina and Taylor 1983; Zhao et al. 1987, 1989, 1992, 1995; Zhao and Valliappan 1991, 1993a, b, c, d, e) is more appropriate because of the following two main reasons: (1) both geometrical irregularities and material complexities in the near field of a system can be simulated using finite elements; and (2) the infinite extension of the system can be effectively and efficiently simulated using infinite elements. For simulating static and dynamic problems, both static and dynamic infinite elements have been developed during the past few decades (Beer and Meek 1981; Zhang and Zhao 1987; Valliappan and Zhao 1992; Zhao et al. 1991, 1992). Since the displacement decay function and wave propagation function are independent of time, both static and dynamic infinite elements can be considered as time-independent infinite elements. For simulating transient pore-fluid flow, heat transfer and mass transport in fluid-saturated porous media of infinite domains, Zhao and Valliappan (1993g, h, 1994a) developed transient infinite elements, in which a time variable is explicitly considered.

In this chapter, two-dimensional mapped transient infinite elements are presented for simulating contaminant transport problems in fractured porous media of infinite domains. To investigate the coupling effect between porous blocks and fissured networks, various parameters, such as contaminant transmissive coefficients between porous blocks and fissured networks, porosities, dispersion coefficients and pore-fluid velocities, are considered in the coupled computational model of finite elements and transient infinite elements. Since the mass transport function of the transient infinite element explicitly depends on both time and space variables, transient contaminant transport processes can be rigorously simulated using the coupled computational model of finite elements and transient infinite elements for simulating fractured porous media of infinite domains.

8.1 Coupled Computational Method of Finite Elements and Transient Infinite Elements for Simulating Transient Contaminant Transport Problems in Fractured Porous Media of Infinite Domains

If advection plays a predominant role in a mass transport problem, the conventional Galerkin finite element method fails in solving the problem so that the resulting solution exhibits pronounced oscillatory behaviour and excessive numerical dispersion. Although a drastic refinement of the finite element mesh can be used to avoid such unwanted oscillatory behaviour and numerical dispersion, it is very inefficient, from the computational point of view. To overcome this problem, the upwind finite element scheme is usually used in the finite element analysis of advection-dominated mass transport problems (Heinrich et al. 1977;

Huyakorn 1977; Huyakorn and Nilkuha 1979). This scheme differs from the conventional Galerkin finite element scheme in the following two aspects: (1) spatial discretization is performed through a general weighted residual technique that employs asymmetrical weighting functions and yields an upwind weighting effect for the advection term of a mass transport equation; (2) the time derivative term of the mass transport equation is weighted using the standard trial functions of symmetrical nature. For this reason, the upwind finite element scheme is used to derive the related formulation for simulating contaminant transport problems in fractured porous media of infinite domains.

8.1.1 Upwind Finite Element Formulation of the Problem

Supposing the principal directions of a double porosity medium are parallel to those of the x and y axes in a global coordinate system, the governing equations of a contaminant transport problem in the double porosity medium with a uniform pore-fluid flow field can be expressed as follows (Barenblatt et al. 1960; Duguid and Lee 1977; Valliappan and Naghadah 1990; Zhao and Valliappan 1994b):

$$D_{1x}\frac{\partial^2 C_1}{\partial x^2} + D_{1y}\frac{\partial^2 C_1}{\partial y^2} - \overline{V}_{1x}\frac{\partial C_1}{\partial x} - \overline{V}_{1y}\frac{\partial C_1}{\partial y} = \frac{\partial C_1}{\partial t} + \frac{1}{\phi_1}\Gamma, \tag{8.1}$$

$$D_{2x}\frac{\partial^2 C_2}{\partial x^2} + D_{2y}\frac{\partial^2 C_2}{\partial y^2} - \overline{V}_{2x}\frac{\partial C_2}{\partial x} - \overline{V}_{2y}\frac{\partial C_2}{\partial y} = \frac{\partial C_2}{\partial t} - \frac{1}{\phi_2}\Gamma, \tag{8.2}$$

where D_{1x} and D_{1y} are the dispersion coefficients of contaminant for the porous block in the x and y directions; D_{2x} and D_{2y} are the dispersion coefficients of contaminant for the fissured network in the x and y directions; $\overline{V}_{1x}$ and $\overline{V}_{1y}$ are the average linear velocities, which are averaged by the pore space (Bear 1972), of the pore-fluid flow within the porous block in the x and y directions; $\overline{V}_{2x}$ and $\overline{V}_{2y}$ are the average linear velocities of the pore-fluid flow within the fissured network; C_1 and C_2 are the contaminant concentrations of the porous block and fissured network, respectively; Γ is a leakage term to express mass exchange between the porous block and the fissured network; ϕ_1 and ϕ_2 are the porosities of the porous block and fissured network.

From the mass conservation law, the leakage term, Γ, can be expressed as

$$\Gamma = \chi\,(\phi_1 C_1 - \phi_2 C_2)\,sign\,(C_1 - C_2)\,sign\,(\phi_1 C_1 - \phi_2 C_2)\,, \tag{8.3}$$

where χ is a transmissive coefficient expressing the contaminant concentration exchange per unit concentration between the porous block and the fissured network per unit time. It has a dimension of $1/s$. $\chi = 0$ means that there is no exchange between the porous block and the fissured network, while $\chi = 1$ means that maximum exchange takes place between the porous block and the fissured network.

Note that Eq. (8.3) always expresses the contaminant transmission from a high-concentration to a low-concentration region. For example, if the concentration in the porous block is greater than that in the fissured network, the contaminant will transmit from the porous block to the fissured network and vice versa. This process is guaranteed by the product of $sign\,(C_1 - C_2)$ and $sign\,(\phi_1 C_1 - \phi_2 C_2)$, even though the porosities of both the porous block and the fissured network are involved. To facilitate computation and to express the formulations concisely, the average contaminant concentrations of a finite element, $\overline{C}_1$ and $\overline{C}_2$, are used instead of C_1 and C_2 in Eq. (8.3). This leads to the following equation:

$$G\left(\overline{C}_1, \overline{C}_2, \phi_1, \phi_2\right) = sign\left(\overline{C}_1 - \overline{C}_2\right) sign\left(\phi_1 \overline{C}_1 - \phi_2 \overline{C}_2\right). \tag{8.4}$$

Equation (8.4) indicates that the value of function G is equal to 1, 0 or –1, depending on the values of $\overline{C}_1$, $\overline{C}_2$, ϕ_1 and ϕ_2.

8.1.1.1 Spatial Discretization of the Problem

In the upwind finite element scheme (Heinrich et al. 1977; Huyakorn 1977; Huyakorn and Nilkuha 1979), the dispersion and advection terms of the transient mass transport equations are weighted using asymmetrical weighting functions to avoid oscillatory solutions, while the time derivative term and transmissive term are weighted using conventional shape functions. Based on this idea, Eqs. (8.1) and (8.2) can be rewritten for an element as follows (Zhao and Valliappan 1994b):

$$\begin{aligned} \iint_A [W]_1^T \left[D_{1x}\frac{\partial^2 C_1}{\partial x^2} + D_{1y}\frac{\partial^2 C_1}{\partial y^2} - \overline{V}_{1x}\frac{\partial C_1}{\partial x} - \overline{V}_{1y}\frac{\partial C_1}{\partial y} \right] dA \\ - \iint_A [N]^T \left[\frac{\partial C_1}{\partial t} + \frac{G}{\phi_1}\chi\,(\phi_1 C_1 - \phi_2 C_2) \right] dA = 0 \end{aligned}, \tag{8.5}$$

$$\begin{aligned} \iint_A [W]_2^T \left[D_{2x}\frac{\partial^2 C_2}{\partial x^2} + D_{2y}\frac{\partial^2 C_2}{\partial y^2} - \overline{V}_{2x}\frac{\partial C_2}{\partial x} - \overline{V}_{2y}\frac{\partial C_2}{\partial y} \right] dA \\ - \iint_A [N]^T \left[\frac{\partial C_2}{\partial t} - \frac{G}{\phi_2}\chi\,(\phi_1 C_1 - \phi_2 C_2) \right] dA = 0 \end{aligned}, \tag{8.6}$$

where A is the area of the element; $[W]_1$ and $[W]_2$ are the non-symmetrical weighting function matrices of the element for the porous block and fissured network, respectively; C_1 and C_2 are the trial functions of the element for the porous block and fissured network. They can be expressed as the functions of nodal concentrations of the element in the finite element sense.

$$C_i = [N]\,\{C_i\}^e \qquad (i = 1, 2), \tag{8.7}$$

where $[N]$ is the conventional shape-function matrix of the element; $\{C_1\}^e$ and $\{C_2\}^e$ are the nodal concentration vectors of the element for the porous block and fissured network at a given time.

Through integrating by parts and applying Green's theorem to the second-order derivatives, Eqs. (8.5) and (8.6) can be written as follows:

$$\left([E_1]^e + [H_1]^e\right)\{C_1\}^e + \frac{G\chi}{\phi_1}[Q_1]^e\left(\phi_1[C_1]^e - \phi_2[C_2]^e\right) + [R_1]^e\left\{\frac{\partial C_1}{\partial t}\right\}^e = \{f_1\}^e, \tag{8.8}$$

$$\left([E_2]^e + [H_2]^e\right)\{C_2\}^e - \frac{G\chi}{\phi_2}[Q_2]^e\left(\phi_1[C_1]^e - \phi_2[C_2]^e\right) + [R_2]^e\left\{\frac{\partial C_2}{\partial t}\right\}^e = \{f_2\}^e, \tag{8.9}$$

where

$$[E_i]^e = \iint_A \left[D_{ix}\frac{\partial[W]_i^T}{\partial x}\frac{\partial[N]}{\partial x} + D_{iy}\frac{\partial[W]_i^T}{\partial y}\frac{\partial[N]}{\partial y}\right]dA \qquad (i = 1,2), \tag{8.10}$$

$$[H_i]^e = \iint_A \left[\overline{V}_{ix}[W]_i^T\frac{\partial[N]}{\partial x} + \overline{V}_{iy}[W]_i^T\frac{\partial[N]}{\partial y}\right]dA \qquad (i = 1,2), \tag{8.11}$$

$$[Q_i]^e = \iint_A \left([N]^T[N]\right)dA \qquad (i = 1,2), \tag{8.12}$$

$$[R_i]^e = \iint_A \left([N]^T[N]\right)dA \qquad (i = 1,2), \tag{8.13}$$

$$\{f_i\}^e = \int_S [W]_i^T\left(D_{ix}\frac{\partial C_1}{\partial x}n_x + D_{iy}\frac{\partial C_2}{\partial y}n_y\right)dS \qquad (i = 1,2), \tag{8.14}$$

where A is the area of the element; S is the boundary line of the element; n_x and n_y are the direction cosines of the outward unit normal vector on the boundary of the element.

Since Eqs. (8.10), (8.11), (8.12), (8.13) and (8.14) are equally valid for both finite and transient infinite elements, the corresponding global matrix can be obtained using the standard assembly procedure in the finite element method (Zienkiewicz 1977). As a result, the global matrix equations for the problem can be expressed as follows:

$$[A_1]\{C_1\} - \frac{G\chi\phi_2}{\phi_1}[Q_1]\{C_2\} + [R_1]\left\{\frac{\partial C_1}{\partial t}\right\} = \{f_1\}, \tag{8.15}$$

$$[A_2]\{C_2\} - \frac{G\chi\phi_1}{\phi_2}[Q_2]\{C_1\} + [R_2]\left\{\frac{\partial C_2}{\partial t}\right\} = \{f_2\}, \tag{8.16}$$

where

$$[A_1] = [E_1] + [H_1] + G\chi[Q_1], \tag{8.17}$$

$$[A_2] = [E_2] + [H_2] + G\chi[Q_2]. \tag{8.18}$$

Since Eqs. (8.15) and (8.16) are coupled by the exchange term, they are better written in the matrix form:

$$[A]\{C\} + [R]\left\{\frac{\partial C}{\partial t}\right\} = \{f\}, \tag{8.19}$$

where

$$[A] = \begin{bmatrix} [A_1] & -\frac{G\chi\phi_2}{\phi_1}[Q_1] \\ -\frac{G\chi\phi_1}{\phi_2}[Q_2] & [A_2] \end{bmatrix}, \tag{8.20}$$

$$[R] = \begin{bmatrix} [R_1] & 0 \\ 0 & [R_2] \end{bmatrix}, \tag{8.21}$$

$$\{C\} = \begin{Bmatrix} \{C_1\} \\ \{C_2\} \end{Bmatrix}, \tag{8.22}$$

$$\{f\} = \begin{Bmatrix} \{f_1\} \\ \{f_2\} \end{Bmatrix}. \tag{8.23}$$

Note that $[A]$ is an asymmetrical matrix due to the consideration of advective pore-fluid flow and the use of asymmetrical weighting functions in formulating the property matrices of the upwind finite element. On the other hand, since $[A]$ and $[R]$ are assembled by both finite elements and transient infinite elements, they are time-dependent matrices and need to be evaluated at any time of interest.

8.1.1.2 Temporal Discretization of the Problem

The solution of Eq. (8.19) in the time domain can be carried out using the finite difference approach for $\{\partial C/\partial t\}$ as follows:

$$\left\{\frac{\partial C}{\partial t}\right\} = \frac{1}{\Delta t}\left(\{C\}^{t+\Delta t} - \{C\}^{t}\right), \tag{8.24}$$

where the superscript represents the time level and Δt is the time step. In the process of solving transient contaminant transport problems using the upwind finite element scheme, both the element size, Δl, and the time step, Δt, need to be selected in such a way that the resulting value of the Courant number ($Cr = V_{\max}\Delta t/\Delta l$) is less than 2.

After the finite difference approach is used for the first derivative of contaminant concentration with respect to time, it is necessary to determine the time level in a time interval between t and $t + \Delta t$, at which the value of the contaminant concentration is evaluated. Generally, the nodal contaminant concentration vector, $\{C\}$, can be approximated anywhere between t and $t + \Delta t$.

$$\{C\} = (1-\alpha)\{C\}^{t} + \alpha\{C\}^{t+\Delta t}, \tag{8.25}$$

where $0 \leq \alpha \leq 1$. If $\alpha = 1$, the solution scheme is fully implicit, while if $\alpha = 0$, the solution scheme is fully explicit. If $\{C\}$ is approximated at a time, $t + (\Delta t/2)$, Eq. (8.19) can be rewritten as follows:

$$\left(\frac{1}{2}[A] + \frac{1}{\Delta t}[R]\right)\{C\}^{t+\Delta t} = \left(\frac{1}{\Delta t}[R] - \frac{1}{2}[A]\right)\{C\}^{t} + \{f\}^{t+(\Delta t/2)}. \tag{8.26}$$

8.1.1.3 Weighting and Shape Functions of the Upwind Finite Element

For a two-dimensional four-node finite element shown in Fig. 8.1, the conventional shape function of the element is well known (Zienkiewicz 1977). The asymmetrical weighting functions for each node of the element can be expressed by the following equations (Zhao and Valliappan 1994b; Zhao et al. 1994):

$$W_{1i} = \frac{1}{16}\left[(1+\xi)\left(-3\overline{\alpha}_{2i}\xi + 3\overline{\alpha}_{2i} + 2\right)\right] \left[(1+\eta)\left(-3\overline{\beta}_{1i}\eta + 3\overline{\beta}_{1i} + 2\right)\right] \quad (i = 1, 2), \tag{8.27}$$

$$W_{2i} = \frac{1}{16}\left[(1+\xi)\left(3\overline{\alpha}_{2i}\xi - 3\overline{\alpha}_{2i} - 2\right) + 4\right] \left[(1+\eta)\left(-3\overline{\beta}_{2i}\eta + 3\overline{\beta}_{2i} + 2\right)\right] \quad (i = 1, 2), \tag{8.28}$$

$$W_{3i} = \frac{1}{16}\left[(1+\xi)\left(3\overline{\alpha}_{1i}\xi - 3\overline{\alpha}_{1i} - 2\right) + 4\right] \left[(1+\eta)\left(3\overline{\beta}_{2i}\eta - 3\overline{\beta}_{2i} - 2\right) + 4\right] \quad (i = 1, 2), \tag{8.29}$$

$$W_{4i} = \frac{1}{16}\left[(1+\xi)\left(-3\overline{\alpha}_{1i}\xi + 3\overline{\alpha}_{1i} + 2\right)\right] \left[(1+\eta)\left(3\overline{\beta}_{1i}\eta - 3\overline{\beta}_{1i} - 2\right) + 4\right] \quad (i = 1, 2), \tag{8.30}$$

where W_{11}, W_{21}, W_{31} and W_{41} are the weighting functions of nodes 1, 2, 3 and 4 of the element for the porous block; W_{12}, W_{22}, W_{32} and W_{42} are the weighting functions of nodes 1, 2, 3 and 4 of the element for the fissured network; ξ and η

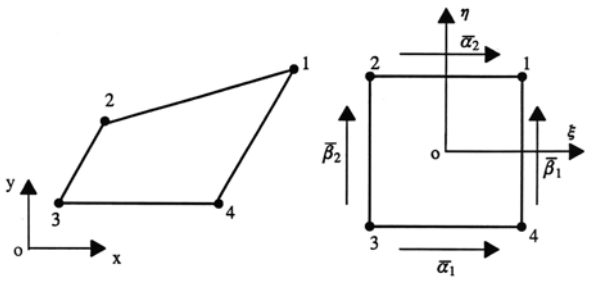

Fig. 8.1 Definition of a four-node upwind finite element

are the local isoparametric coordinates of the element; $\overline{\alpha}_{11}$, $\overline{\beta}_{11}$, $\overline{\alpha}_{21}$ and $\overline{\beta}_{21}$ are the upwind parameters corresponding with sides 3-4, 4-1, 2-1 and 3-2 of the element for the porous block; $\overline{\alpha}_{12}$, $\overline{\beta}_{12}$, $\overline{\alpha}_{22}$ and $\overline{\beta}_{22}$ are the upwind parameters corresponding with sides 3-4, 4-1, 2-1 and 3-2 of the element for the fissured network.

For the upwind finite element scheme, the signs of these upwind parameters depend on the signs of the average pore-fluid flow velocities of the element sides, representing the advective flow direction associated with the contaminant transport process in the fractured porous medium. For this reason, these upwind parameters are expressed as

$$\overline{\alpha}_{ij} = \alpha_{ij}^{opt} sign\left(\overline{V}_j\right) \qquad (i = 1, 2; j = 1, 2), \tag{8.31}$$

$$\overline{\beta}_{ij} = \beta_{ij}^{opt} sign\left(\overline{V}_j\right) \qquad (i = 1, 2; j = 1, 2), \tag{8.32}$$

where α_{ij}^{opt} and β_{ij}^{opt} $(i = 1, 2; j = 1, 2)$ are the optimal values of the upwind parameters for the related element sides; $\overline{V}_1$ is the corresponding average speed of pore-fluid flow along the element side for the porous block; $\overline{V}_2$ is the corresponding average speed of pore-fluid flow along the element side for the fissured network; $\overline{V}_1$ and $\overline{V}_2$ can be determined using the following formulas:

$$\overline{V}_1 = \frac{1}{2}\left(\vec{V}_{1p} + \vec{V}_{1q}\right) \bullet \vec{I}_{pq}, \tag{8.33}$$

$$\overline{V}_2 = \frac{1}{2}\left(\vec{V}_{2p} + \vec{V}_{2q}\right) \bullet \vec{I}_{pq}, \tag{8.34}$$

where p and q are the node numbers of an element side; $\vec{V}_{1p}$ and $\vec{V}_{1q}$ are the velocity vectors of nodes p and q of the element for the porous block; $\vec{V}_{2p}$ and $\vec{V}_{2q}$ are the velocity vectors of nodes p and q of the element for the fissured network; $\vec{I}_{pq}$ is the direction vector of the element side in the local coordinate system with the same positive direction as that of the local coordinate system of the element.

The optimal values of upwind parameters depend on the Courant number of the element side and can be determined using the following equations (Huyakorn and Nilkuha 1979; Zhao et al. 1994):

$$\alpha_{ij}^{opt} = \coth\left(\frac{\left|\overline{V}_j\right| \Delta l}{2D_{ix}}\right) - \frac{2D_{ix}}{\left|\overline{V}_j\right| \Delta l} \qquad (i = 1, 2; j = 1, 2), \tag{8.35}$$

$$\beta_{ij}^{opt} = \coth\left(\frac{\left|\overline{V}_j\right| \Delta l}{2D_{iy}}\right) - \frac{2D_{iy}}{\left|\overline{V}_j\right| \Delta l} \qquad (i = 1, 2; j = 1, 2), \tag{8.36}$$

where coth stands for the hyperbolic cotangent function; Δl is the characteristic length of the element.

To obtain satisfactory solutions, the derivatives, $\partial W_{ij} \big/ \partial \xi$ and $\partial W_{ij} \big/ \partial \eta$ $(i = 1, 2, 3, 4; j = 1, 2)$, of the element need to be evaluated in such a way that when

differentiation is taken with respect to one particular coordinate variable, the values of the upwind parameters along the remaining coordinate variables must be set to zero. Thus, the derivatives of the upwind weighting functions of the element can be expressed as follows:

$$\frac{\partial W_{1i}}{\partial \xi} = -\frac{1}{4}(1+\eta)\ (3\overline{\alpha}_{2i}\xi - 1) \qquad (i = 1, 2), \tag{8.37}$$

$$\frac{\partial W_{2i}}{\partial \xi} = \frac{1}{4}(1+\eta)\ (3\overline{\alpha}_{2i}\xi - 1) \qquad (i = 1, 2), \tag{8.38}$$

$$\frac{\partial W_{3i}}{\partial \xi} = \frac{1}{4}(1-\eta)\ (3\overline{\alpha}_{1i}\xi - 1) \qquad (i = 1, 2), \tag{8.39}$$

$$\frac{\partial W_{4i}}{\partial \xi} = -\frac{1}{4}(1-\eta)\ (3\overline{\alpha}_{1i}\xi - 1) \qquad (i = 1, 2), \tag{8.40}$$

$$\frac{\partial W_{1i}}{\partial \eta} = -\frac{1}{4}(1+\xi)\left(3\overline{\beta}_{1i}\eta - 1\right) \qquad (i = 1, 2), \tag{8.41}$$

$$\frac{\partial W_{2i}}{\partial \eta} = -\frac{1}{4}(1-\xi)\left(3\overline{\beta}_{2i}\eta - 1\right) \qquad (i = 1, 2), \tag{8.42}$$

$$\frac{\partial W_{3i}}{\partial \eta} = \frac{1}{4}(1-\xi)\left(3\overline{\beta}_{2i}\eta - 1\right) \qquad (i = 1, 2), \tag{8.43}$$

$$\frac{\partial W_{4i}}{\partial \eta} = \frac{1}{4}(1+\xi)\left(3\overline{\beta}_{1i}\eta - 1\right) \qquad (i = 1, 2). \tag{8.44}$$

If the conventional mapping technique for isoparametric elements is used, substituting the asymmetrical upwind weighting functions and conventional shape functions of the element into Eqs. (8.10), (8.11), (8.12) and (8.13) yields the following property matrices of the proposed upwind finite element for simulating transient contaminant transport problems in double porosity media:

$$[E_i]^e = \int_{-1}^{1}\int_{-1}^{1}\left(D_{ix}\frac{\partial\,[W]_i^T}{\partial x}\frac{\partial\,[N]}{\partial x} + D_{iy}\frac{\partial\,[W]_i^T}{\partial y}\frac{\partial\,[N]}{\partial y}\right)|J|\,d\xi\,d\eta \quad (i = 1, 2), \tag{8.45}$$

$$[H_i]^e = \int_{-1}^{1}\int_{-1}^{1}\left(\overline{V}_{ix}\,[W]_i^T\,\frac{\partial\,[N]}{\partial x} + \overline{V}_{iy}\,[W]_i^T\,\frac{\partial\,[N]}{\partial y}\right)|J|\,d\xi\,d\eta \quad (i = 1, 2), \tag{8.46}$$

$$[Q_i]^e = \int_{-1}^{1}\int_{-1}^{1}\left([N]^T\,[N]\right)|J|\,d\xi\,d\eta \qquad (i = 1, 2), \tag{8.47}$$

$$[R_i]^e = \int_{-1}^{1}\int_{-1}^{1}\left([N]^T\,[N]\right)|J|\,d\xi\,d\eta \qquad (i = 1, 2), \tag{8.48}$$

where $|J|$ is the Jacobian determinant of the upwind finite element.

8.1.2 Fundamental Formulas of Mapped Transient Infinite Elements for Simulating Transient Contaminant Transport Problems

To illustrate the fundamental concept of transient infinite elements, a one-dimensional contaminant transport problem in a fluid-saturated porous medium of an infinite domain is considered in this subsection. Supposing that a unit point contaminant concentraction exists at $x = 0$ and a unidirectional pore-fluid flow is along the positive direction of the x axis, both advection and dispersion will take place from the origin of the x axis ($x = 0$) to the far field of the system. The governing equation for the resulting one-dimensional transient contaminant transport problem in a fluid-saturated porous medium can be expressed as

$$\frac{\partial C}{\partial t} = D_x \frac{\partial^2 C}{\partial x^2} - \overline{V}_x \frac{\partial C}{\partial x}, \tag{8.49}$$

where D_x is the dispersion coefficient of contaminant in the x direction; $\overline{V}_x$ is the average linear velocity of the unidirectional pore-fluid flow; C is the contaminant concentration in the fluid-saturated porous medium.

Since Eq. (8.49) is one-dimensional in space, the analytical solution for this equation with D_x and $\overline{V}_x$ constant and a given initial contaminant concentration at the origin of the global coordinate system is available (Ogata and Banks 1961).

$$C(x,t) = \frac{C_0}{\sqrt{4\pi D_x t}} \exp\left[-\frac{(x - \overline{V}_x t)^2}{4D_x t}\right], \tag{8.50}$$

where C_0 is the concentration of the point contaminant source at the origin of the global coordinate system.

For a typical one-dimensional transient infinite element shown in Fig. 8.2, the global coordinate of node 1 is x_1 and the local coordinate of this node is identical to zero. The contaminant concentration at this node for a given time, t, can be expressed as follows:

$$C(x_1,t) = \frac{C_0}{\sqrt{4\pi D_x t}} \exp\left[-\frac{(x_1 - \overline{V}_x t)^2}{4D_x t}\right]. \tag{8.51}$$

For any point within this one-dimensional transient infinite element, taking $x = x_1 + \Delta x$ as an example, the contaminant concentration of this point can be derived from Eq. (8.51).

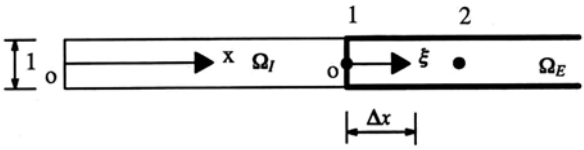

Fig. 8.2 One-dimensional mapped transient infinite elements

$$C(x_1 + \Delta x, t) = C(x_{1,}\, t) \exp\left[-\frac{\Delta x^2 + 2\Delta x(x_1 - \overline{V}_x t)}{4D_x t}\right]. \tag{8.52}$$

Considering the fact that $\xi = \Delta x$ for this one-dimensional transient infinite element, the mass transport function of this element can be expressed as

$$F_{mt}(\xi, t) = \exp\left[-\frac{\xi^2 + 2(x_1 - \overline{V}_x t)\xi}{4D_x t}\right]. \tag{8.52}$$

As a result, the contaminant concentration field within the one-dimensional transient infinite element can be expressed in the form:

$$C\,(\xi,t) = C_1 F_{mt}\,(\xi,t) = C_1 N_1, \tag{8.54}$$

where C_1 is the nodal contaminant concentration of the one-dimensional transient infinite element; C is the contaminant concentration within the one-dimensional transient infinite element; N_1 is the shape function of the one-dimensional transient infinite element. Note that the mass transport function of the transient infinite element is identical to the shape function for simulating one-dimensional transient contaminant transport problems.

Figures 8.3 and 8.4 show the distributions of the mass transport function for several cases. In these figures, $\overline{V}_x = 0$ and $\overline{V}_x = 0.1\ \mathrm{m\,d^{-1}}$ are considered to illustrate the effects of the pore-fluid flow velocity on the distribution of the mass transport function. Not only can both the dispersion coefficient and the pore-fluid flow velocity have considerable influences on the distribution of the mass transport function, but also the time in the analysis can have a significant effect on the distribution of the mass transport function of the transient infinite element. It is the explicit consideration of the effect of a time variable that determines the characteristic of the proposed transient infinite element. On the other hand, since the mass transport function of the transient infinite element explicitly depends on time, it can be concluded that the time effect should be considered in the process of constructing transient infinite elements for simulating various transient problems. Otherwise, errors in the corresponding numerical simulation will inevitably occur.

The above procedure, associated with the one-dimensional transient infinite element, can be extended to the construction of two-dimensional transient infinite elements for simulating transient contaminant transport problems in fractured porous media of infinite domains (Zhao and Valliappan 1994b). If the near field of an infinite domain system is appropriately chosen, the leakage effect between the porous block and the fissured network in the far field of the system may become negligible as a result of the term, $\phi_1 C_1 - \phi_2 C_2$ in Eq. (8.3), approaching zero. In this case, the mass transport functions of a transient infinite element can be expressed as

$$F_{1mt}(\xi,t) = \exp\left[-\frac{\xi^2 + 2(x_1 - \overline{V}_{1\xi} t)\xi}{4D_{1\xi} t}\right], \tag{8.55}$$

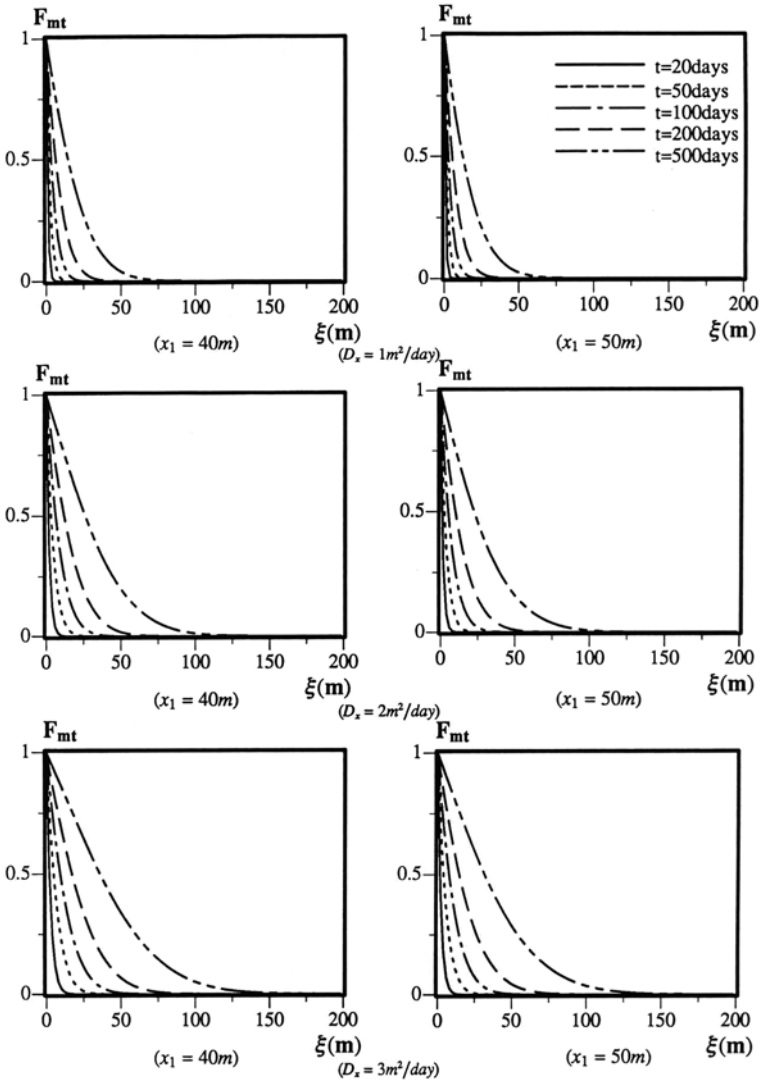

Fig. 8.3 Distributions of mass transport functions of the transient infinite element ($\overline{V}_x = 0$)

$$F_{2mt}(\xi,t) = \exp\left[-\frac{\xi^2 + 2(x_1 - \overline{V}_{2\xi}t)\xi}{4D_{2\xi}t}\right], \tag{8.56}$$

where F_{1mt} and F_{2mt} are the mass transport functions of the transient infinite element for the porous block and fissured network, respectively; $\overline{V}_{1\xi}$ and $\overline{V}_{2\xi}$ are the average linear pore-fluid flow velocities in the ξ direction of the local coordinate system; $D_{1\xi}$ and $D_{2\xi}$ are the dispersion coefficients in the ξ direction of the local coordinate system.

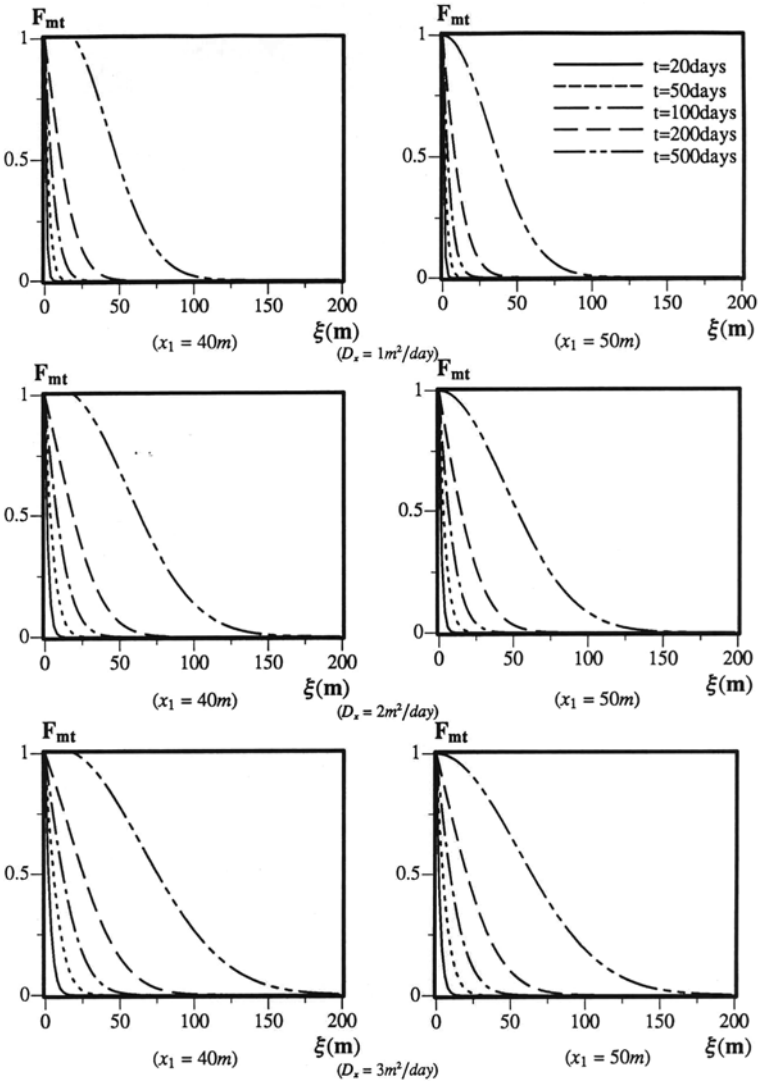

Fig. 8.4 Distributions of mass transport functions of the transient infinite element ($\overline{V}_x = 0.1\,\mathrm{m\,d^{-1}}$)

Based on the mass transport functions of transient infinite elements, the contaminant concentration shape function matrix of a two-dimensional transient infinite element can be derived (Zhao and Valliappan 1994b). Figure 8.5 shows a two-dimensional four-node transient infinite element, for which the mapping relationship between the global and local coordinate systems can be expressed as

$$x = \sum_{i=1}^{4} M_i x_i, \tag{8.57}$$

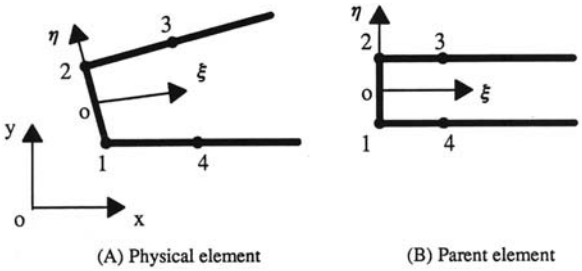

Fig. 8.5 Two-dimensional mapped transient infinite elements

$$y = \sum_{i=1}^{4} M_i y_i, \tag{8.58}$$

where M_i is the mapping function at each node of the element, viz.,

$$M_1 = \frac{1}{2}(1-\xi)(1-\eta), \tag{8.59}$$

$$M_2 = \frac{1}{2}(1-\xi)(1+\eta), \tag{8.60}$$

$$M_3 = \frac{1}{2}\xi(1+\eta), \tag{8.61}$$

$$M_4 = \frac{1}{2}\xi(1-\eta). \tag{8.62}$$

The contaminant concentration field within the two-dimensional transient infinite element shown in Fig. 8.5 can be defined as

$$C_i = \sum_{j=1}^{2} \hat{N}_{ji} C_{ji} = [\hat{N}]_i \begin{Bmatrix} C_{1i} \\ C_{2i} \end{Bmatrix} \qquad (i = 1, 2), \tag{8.63}$$

where C_1 and C_2 are the contaminant concentrations for the porous block and fissured network; $\left[\hat{N}\right]_1$ and $\left[\hat{N}\right]_2$ are the shape function matrices of the two-dimensional transient infinite element for the porous block and fissured network; $\hat{N}_{1i}$ and $\hat{N}_{2i}$ $(i = 1, 2)$ are the shape functions of nodes 1 and 2 for the porous block and fissured network, respectively.

$$\hat{N}_{1i} = \frac{1}{2} F_{imt}(\xi, t)(1-\eta) \qquad (i = 1, 2), \tag{8.64}$$

$$\hat{N}_{2i} = \frac{1}{2} F_{imt}(\xi, t)(1+\eta) \qquad (i = 1, 2). \tag{8.65}$$

Since the number of nodes used for the definition of the shape of the two-dimensional transient infinite element is greater than that used for defining the

contaminant concentration field of the two-dimensional transient infinite element, the corresponding two-dimensional parent transient infinite element is a superparametric element.

Based on the same procedures as those used in the conventional finite element method (Zienkiewicz 1977; Zhao and Valliappan 1994b), the property matrices of this two-dimensional transient infinite element can be expressed as

$$[\hat{E}_i]^e = \int_0^{\infty}\int_{-1}^{1}\left(D_{ix}\frac{\partial[\hat{W}]_i^T}{\partial x}\frac{\partial[\hat{N}]_i}{\partial x} + D_{iy}\frac{\partial[\hat{W}]_i^T}{\partial y}\frac{\partial[\hat{N}]_i}{\partial y}\right)|J|\,d\eta d\xi \qquad (i=1,2), \tag{8.66}$$

$$[\hat{H}_i]^e = \int_0^{\infty}\int_{-1}^{1}\left(\overline{V}_{ix}[\hat{W}]_i^T\frac{\partial[\hat{N}]_i}{\partial x} + \overline{V}_{iy}[\hat{W}]_i^T\frac{\partial[\hat{N}]_i}{\partial y}\right)|J|\,d\eta d\xi \qquad (i=1,2), \tag{8.67}$$

$$[\hat{Q}_i]^e = [\hat{R}_i]^e = \int_0^{\infty}\int_{-1}^{1}\left([\hat{N}]_i^T[\hat{N}]_i\right)|J|\,d\eta d\xi \qquad (i=1,2), \tag{8.68}$$

$$\left[\hat{N}\right]_i = \left[\hat{N}_{1i} \quad \hat{N}_{2i}\right], \qquad (i=1,2), \tag{8.69}$$

$$\left[\hat{W}\right]_i = \left[\hat{W}_{1i} \quad \hat{W}_{2i}\right], \qquad (i=1,2), \tag{8.70}$$

where $|J|$ is the Jacobian determinant of the two-dimensional transient infinite element.

To reflect the upwind effect for the two-dimensional transient infinite element, the following asymmetric weighting functions are used in evaluating the property matrices of the two-dimensional transient infinite elements:

$$\left[\hat{W}(\xi,\eta,t)\right]_i = \left[\hat{N}(\xi,\eta,t-\Delta t)\right]_i, \qquad (i=1,2), \tag{8.71}$$

By using the variable substitution technique and letting $\xi = (1+\beta)\big/(1-\beta)$, Eqs. (8.66), (8.67) and (8.68) can be rewritten as

$$[\hat{E}_i]_1^e = \int_{-1}^{1}\int_{-1}^{1}\left(D_{ix}\frac{\partial[\hat{W}]_i^T}{\partial x}\frac{\partial[\hat{N}]_i}{\partial x} + D_{iy}\frac{\partial[\hat{W}]_i^T}{\partial y}\frac{\partial[\hat{N}]_i}{\partial y}\right)\frac{2}{(\beta-1)^2}|J|\,d\eta d\beta \ (i=1,2), \tag{8.72}$$

$$[\hat{H}_i]_1^e = \int_{-1}^{1}\int_{-1}^{1}\left(\overline{V}_{ix}[\hat{W}]_i^T\frac{\partial[\hat{N}]_i}{\partial x} + \overline{V}_{iy}[\hat{W}]_i^T\frac{\partial[\hat{N}]_i}{\partial y}\right)\frac{2}{(\beta-1)^2}|J|\,d\eta d\beta \ (i=1,2), \tag{8.73}$$

$$[\hat{Q}_i]_1^e = [\hat{R}_i]_1^e = \int_{-1}^{1}\int_{-1}^{1}\left([\hat{N}]_i^T[\hat{N}]_i\right)\frac{2}{(\beta-1)^2}|J|\,d\eta d\beta \qquad (i=1,2). \tag{8.74}$$

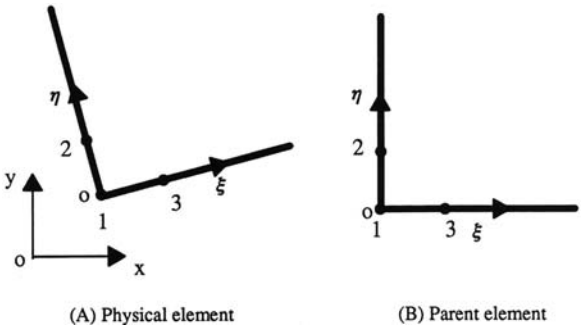

Fig. 8.6 Two-dimensional mapped transient bi-infinite elements

Equations (8.72), (8.73) and (8.74) indicate that the property matrices of the two-dimensional transient infinite element can be evaluated using the Gauss–Legendre integration scheme.

It is noted that under certain situations, a two-dimensional three-node transient bi-infinite element, as shown in Fig. 8.6, can be useful for the numerical analysis. Similarly, the mapping relationship of this two-dimensional three-node transient bi-infinite element can be defined as follows:

$$x = \sum_{i=1}^{3} M_i x_i, \tag{8.75}$$

$$y = \sum_{i=1}^{3} M_i y_i, \tag{8.76}$$

where M_i is the mapping function at each node of the two-dimensional three-node transient bi-infinite element

$$M_1 = (1-\xi)(1-\eta), \tag{8.77}$$

$$M_2 = \frac{1}{2}\xi(1+\eta), \tag{8.78}$$

$$M_3 = \frac{1}{2}(1+\xi)\eta. \tag{8.79}$$

The contaminant concentration shape function of this two-dimensional three-node transient bi-infinite element can be expressed as

$$[\hat{N}]_i = [\hat{N}_1]_i = [F_{imt}(\xi,t)F_{imt}(\eta,t)] \qquad (i=1,2), \tag{8.80}$$

where

$$F_{imt}(\xi,t) = \exp\left[-\frac{\xi^2 + 2(x_1 - \overline{V}_{i\xi}t)\xi}{4D_{i\xi}t}\right] \qquad (i=1,2), \tag{8.81}$$

$$F_{imt}(\eta, t) = \exp\left[-\frac{\eta^2 + 2(y_1 - \overline{V}_{i\eta}t)\eta}{4D_{i\eta}t}\right] \qquad (i = 1, 2). \tag{8.82}$$

Finally, the property matrices of the two-dimensional three-node transient bi-infinite element can be derived (Zhao and Valliappan 1994b).

$$[\hat{E}_i]_2^e = \int_{-1}^{1}\int_{-1}^{1}\left(D_{ix}\frac{\partial[\hat{W}]_i^T}{\partial x}\frac{\partial[\hat{N}]_i}{\partial x} + D_{iy}\frac{\partial[\hat{W}]_i^T}{\partial y}\frac{\partial[\hat{N}]_i}{\partial y}\right) \frac{4}{(\beta-1)^2(\gamma-1)^2}|J|\,d\gamma\,d\beta \qquad (i = 1, 2), \tag{8.83}$$

$$[\hat{H}_i]_2^e = \int_{-1}^{1}\int_{-1}^{1}\left(\overline{V}_{ix}[\hat{W}]_i^T\frac{\partial[\hat{N}]_i}{\partial x} + \overline{V}_{iy}[\overline{W}]_i^T\frac{\partial[\hat{N}]_i}{\partial y}\right) \frac{4}{(\beta-1)^2(\gamma-1)^2}|J|\,d\gamma\,d\beta \qquad (i = 1, 2), \tag{8.84}$$

$$[\hat{Q}_i]_2^e = [\hat{R}_i]_2^e = \int_{-1}^{1}\int_{-1}^{1}\left([\overline{W}]_i^T[\hat{N}]_i\right)\frac{2}{(\beta-1)^2(\gamma-1)^2}|J|\,d\gamma\,d\beta \qquad (i = 1, 2), \tag{8.85}$$

$$\left[\hat{W}(\xi,\eta,t)\right]_i = \left[\hat{N}(\xi,\eta,t-\Delta t)\right]_i, \qquad (i = 1, 2). \tag{8.86}$$

After the property matrices of both upwind finite elements and transient infinite elements are obtained, the coupled computational method of upwind finite elements and transient infinite elements can be used to solve transient contaminant transport problems in fractured porous media of infinite domains. As the present transient infinite element explicitly depends on time, the corresponding property matrices need to be evaluated at each time step in the computation so that the accuracy of numerical results can be ensured for any time of interest.

8.1.3 Verification of the Coupled Computational Method of Upwind Finite Elements and Transient Infinite Elements

The correctness and usefulness of the coupled computational method of upwind finite elements and transient infinite elements can be verified by some simple but critical problems, for which the exact analytical solutions are already available. To examine the two-dimensional behaviour of the proposed transient infinite elements, a fundamental problem with a given contaminant concentration at the centre of a single porosity medium in a horizontal infinite plane is considered in this subsection. This can be carried out by simply setting the exchange term in a double porosity medium to zero so that the double porosity medium can be treated as two overlapping independent media of single porosity. Figure 8.7 shows the discretized

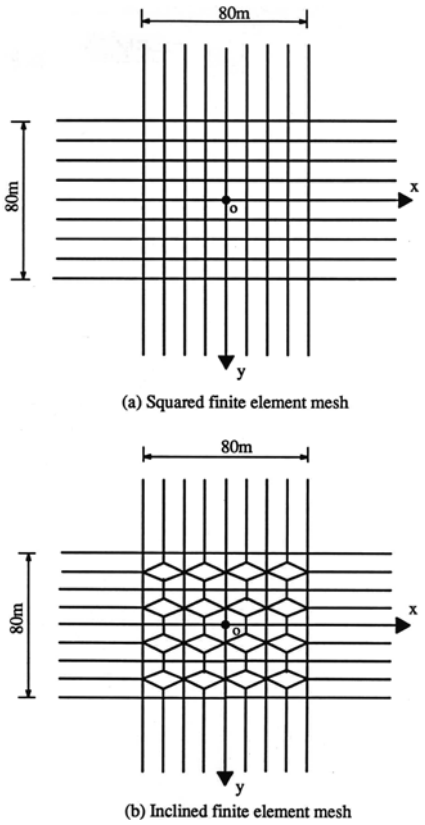

Fig. 8.7 Coupled computational model of a verification problem: (**a**) squared finite element mesh; (**b**) inclined finite element mesh

model of this problem, where the origin of the global coordinate system is subjected to a point contaminant source with the concentration of 100 mg cm^{-3} (i.e. $C_0 = 100$ mg cm^{-3}) at $t = 0$. For the purpose of investigating the effect of the finite element mesh on the numerical results, the near field of the system, which is chosen as 80×80 m, has been simulated by squared regular finite elements (see Fig. 8.7(a)) and by inclined irregular finite elements (see Fig. 8.7(b)). The far field is simulated by two-dimensional transient mapped infinite elements as proposed in this chapter. The following parameters are used in the numerical analysis: the average linear velocities of pore-fluid flow are 0.05 m d^{-1} in the x and y directions; the diffusion/dispersion coefficients are 0.5 m^2 d^{-1} in the x and y directions; the time step used in the computation is 10 days.

Figure 8.8 shows the comparison between the current numerical and the analytical solutions (Lardner and Song 1991). In this figure, the dimensionless concentration distributions of the contaminant in the near field of the first quadrant of the global coordinate system, namely in the region of $40\,\text{m} \geq x \geq 0$ and $40\,\text{m} \geq y \geq 0$, have been displayed at three different time instants. It is noted that, in terms of the numerical solutions shown in Fig. 8.8, the solid lines represent the numerical results obtained by using the mesh of squared regular finite elements, while the

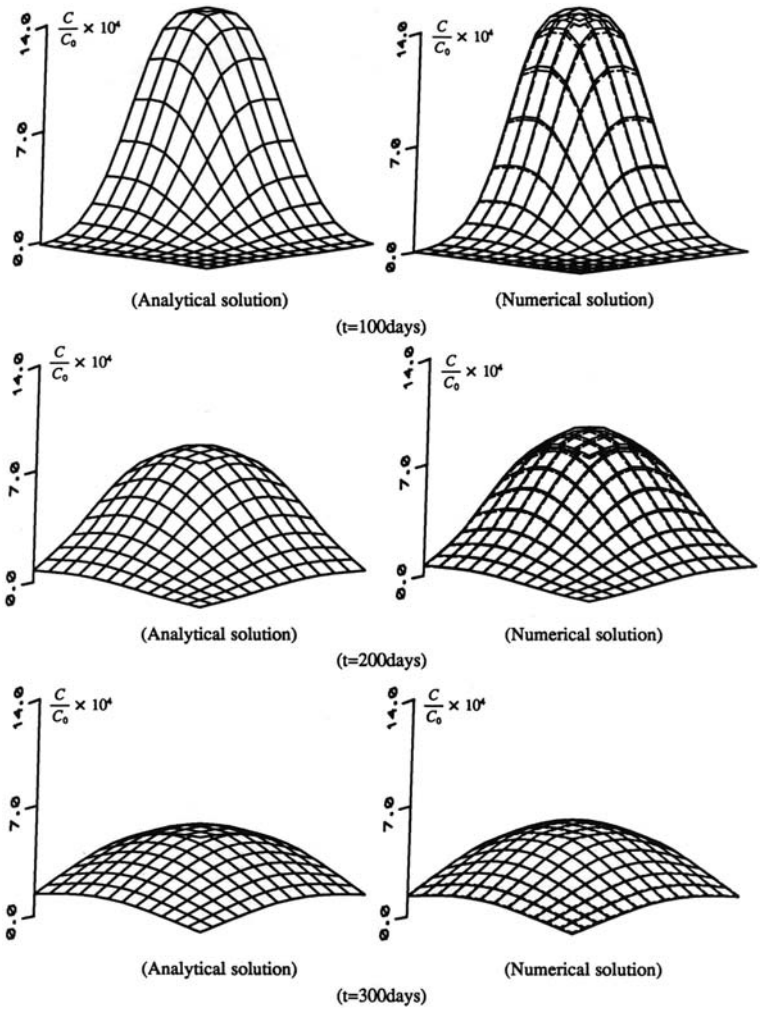

Fig. 8.8 Comparison of numerical results with analytical solutions

dashed lines express the numerical results from using the mesh of inclined irregular finite elements. From this figure, it can be observed that excellent coincidence exists between the current numerical results and the analytical solutions, even though the near field simulated by finite elements is very small. This demonstrates that the coupled computational method of upwind finite elements and transient infinite elements is very useful for the numerical simulation of transient contaminant transport problems in fluid-saturated porous media of infinite domains. In addition, it is clear that the numerical results obtained by using the mesh of the squared regular finite elements yield good agreement with those using the mesh of the inclined irregular finite elements. This illustrates that the coupled method of upwind finite elements

and transient infinite elements can be used to solve transient contaminant transport problems with irregular meshes in the near field of the system.

8.2 Parametric Study of Transient Contaminant Transport Problems in Fractured Porous Media of Infinite Domains

Although the quantitative application of a numerical model to a contaminant transport problem in natural environments is limited by difficulties in determining the values of distributions of appropriate field parameters, a sophisticated numerical model can play a useful role in demonstrating the sensitivity of a contaminant transport process to each of the parameters involved. The resulting information from this kind of study may provide an improved understanding of the effect of each parameter on the contaminant transport process. In this regard, the sophisticated numerical model can lead to greater efficiency and insight in the process of collecting field data. This is the main reason for conducting a parametric study on contaminant transport processes in fractured porous media of infinite domains in this section.

Regarding the determination of material parameters involved in the governing equations of transient contaminant transport problems in fractured porous media, Rowe et al. (1988) proposed some laboratory techniques for assessing the effective matrix porosity so that a reduction in the total porosity obtained by normal geotechnical procedures is considered as a result of the dead-end pores and pores too small to permit contaminant transport. On the other hand, if a fissured network is comprised of three orthogonally intersecting sets of equally spaced, parallel fractures, Rowe and Booker (1989, 1990a, b, 1991) presented the relationships between the fissure spacing and related parameters. The general form of such relationships can be expressed in the x direction as follows:

$$v_{ax} = v_{1x}^{f}\frac{h_1}{H_1} + v_{2x}^{f}\frac{h_2}{H_2}, \tag{8.87}$$

$$D_{ax} = D_{1x}^{f}\frac{h_1}{H_1} + D_{2x}^{f}\frac{h_2}{H_2}, \tag{8.88}$$

$$\phi_f = \frac{h_1}{H_1} + \frac{h_2}{H_2} + \frac{h_3}{H_3}, \tag{8.89}$$

where v_{1x}^{f} and v_{2x}^{f} are the average linear pore-fluid velocities in sets one and two of fissures, the normal of whose surfaces are perpendicular to the x axis; D_{1x}^{f} and D_{2x}^{f} are the corresponding dispersion coefficients of these two sets of fissures; v_{ax} is the Darcy velocity in the x direction; D_{ax} is the apparent dispersion coefficient of the fissured network in the x direction; ϕ_f is the porosity of the fissured network; h_1 and h_2 are the widths of these two sets of fissures under consideration; H_1 and H_2 are the corresponding fissure spacing for these two sets of fissures; h_3 and H_3 are the width and spacing of the third set of fissures, of which the normal surface is parallel to the x axis.

For a two- or three-dimensional contaminant transport problem, similar formulas to those expressed in Eqs. (8.87) and (8.88) can be employed to determine the values of the Darcy velocity and apparent dispersion coefficient of the fissured network in the y and z directions. Since the fissure characteristics of a fissured network can be represented by the parameters such as v_{ax}, D_{ax} and ϕ_f, instead of using the fissure spacing and width directly, average linear pore-fluid velocities, dispersion coefficients and the porosity of the fissured network are used to investigate the effects of the fissured network on transient contaminant transport processes in fractured porous media.

8.2.1 Effects of the Leakage between a Porous Block and a Fissured Network on Contaminant Concentration Distributions in the Fractured Porous Medium

In this subsection, the effects of leakages between porous blocks and fissured networks on contaminant transport processes in fractured porous media of infinite domains are considered using the coupled method of upwind finite elements and transient infinite elements. Such leakage effects reflect the interactions between porous blocks and fissured networks in fractured porous media. From a mathematical point of view, since a distributed contaminant source can be decomposed into a sum of several point contaminant sources, the use of a point contaminant source may be the best choice for investigating the general contaminant transport mechanism in fractured porous media of infinite domains. For this reason, a fundamental mass transport problem with an initial point contaminant source of a given concentration at the centre of a horizontal infinite plane is considered in this subsection.

As shown in Fig. 8.9, the origin of the coordinate system is subjected to a point contaminant source with a concentration of $1\,\mathrm{kg\,m^{-3}}$ at $t = 0$. This means that the initial boundary condition of the problem is $C(x, y, t) = \delta(x)\delta(y)\delta(t)\,\mathrm{kgm^{-3}}$, where δ is the Kronecker delta with a value of either one or zero. The whole problem domain is divided into a near field ($|x|$<100 m, $|y|$<100 m) and a far field ($|x|$>100 m, $|y|$> 100 m), so that the interface between the near field and the far field is presented by the four lines expressed by $x = \pm 100\,\mathrm{m}$ ($|y| \leq 100\,\mathrm{m}$) and $y = \pm 100\,\mathrm{m}$ ($|x| \leq 100\,\mathrm{m}$) in the computational model. The near field of the problem domain is simulated using upwind finite elements, while the far field of the problem domain is simulated using transient infinite elements. To investigate the effect of advective pore-fluid flow on the contaminant transport process in a fractured porous medium, it is assumed that the positive direction of the pore-fluid flow is in coincidence with that of the x axis.

The following parameters are used in the coupled computational model of upwind finite elements and transient infinite elements. For the porous continuum, the average linear velocities of pore-fluid flow are $0.1\,\mathrm{m\,d^{-1}}$ and $0\,\mathrm{m\,d^{-1}}$ in the x and y directions, respectively; the dispersion coefficients are $1\,\mathrm{m^2d^{-1}}$ and $0.1\,\mathrm{m^2d^{-1}}$ in the x and y directions. For the fissured continuum, both the average linear veloc-

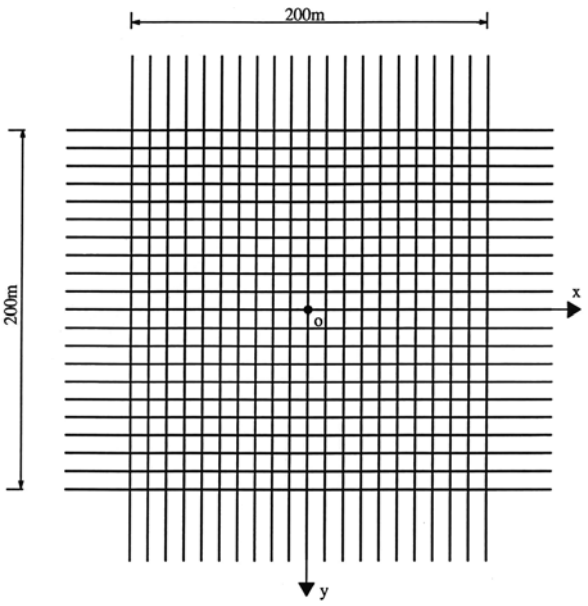

Fig. 8.9 Computational model of contaminant transport in a fractured porous medium: the near field is simulated using finite elements, while the far field is simulated using transient infinite elements

ities of pore-fluid flow and the dispersion coefficients in the x and y directions are exactly the same as those used for the porous continuum. Since only the porosity ratio between the fissured continuum (representing the fissured network) and the porous continuum (representing the porous block) is involved in the governing equations of contaminant transport problems in fractured porous media, which are treated as double porosity continua, the porosity ratio of the fissured continuum to the porous continuum, ϕ_2/ϕ_1, is assumed to be 4, while the porosity of the continuum (i.e. ϕ_1) is 0.05 in the computational model of the overlapping double porosity continua. Regarding the discretization of time, the central difference scheme (Zhao and Valliappan 1994b, c) is used with a time step of $\Delta t = 10$ days. Since the leakage due to the solute diffusion between the porous block and the fissured network can be considered by a transmissive coefficient in the computational model, six different transmissive coefficients between the porous and fissured continua, namely χ =0, 0.001, 0.005, 0.01, 0.1 and 1.0 per unit time, are used to investigate the effects of leakages between the porous block and the fissured network on the contaminant concentration distributions in the fractured porous medium.

Figures 8.10 and 8.11 show the dimensionless concentration distribution of contaminant in the near field of the first quadrant of the fractured porous medium at $t = 100$ and 400 days, respectively. Note that the dimensionless contaminant concentration is defined as $(C/C_0) \times 10^3$. In these figures, Tr is used to represent the transmissive coefficient between the porous and fissured continua so that Tr $= \chi$ in this subsection. The numerical results shown in the left columns are obtained from the porous continuum, which is used to represent the porous block, while the numerical results shown in the right columns are obtained from the fissured

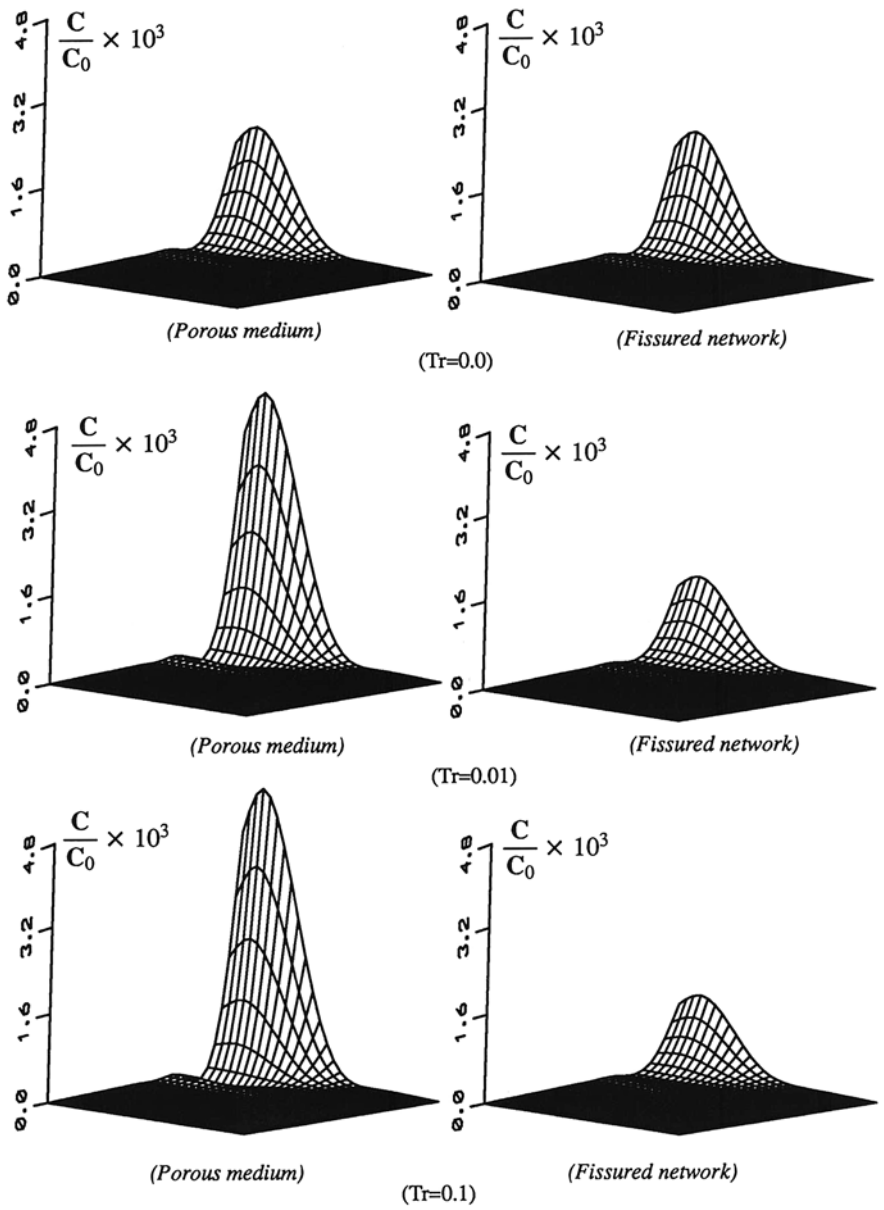

Fig. 8.10 Effects of leakages on dimensionless contaminant distributions in the fractured porous medium (t = 100 days)

continuum, which is used to represent the fissured network of the fractured porous medium. As the strength of the leakage between the porous block and the fissured network can be represented by the value of the transmissive coefficient, the related numerical results indicate that the strength of the leakage has a significant effect on

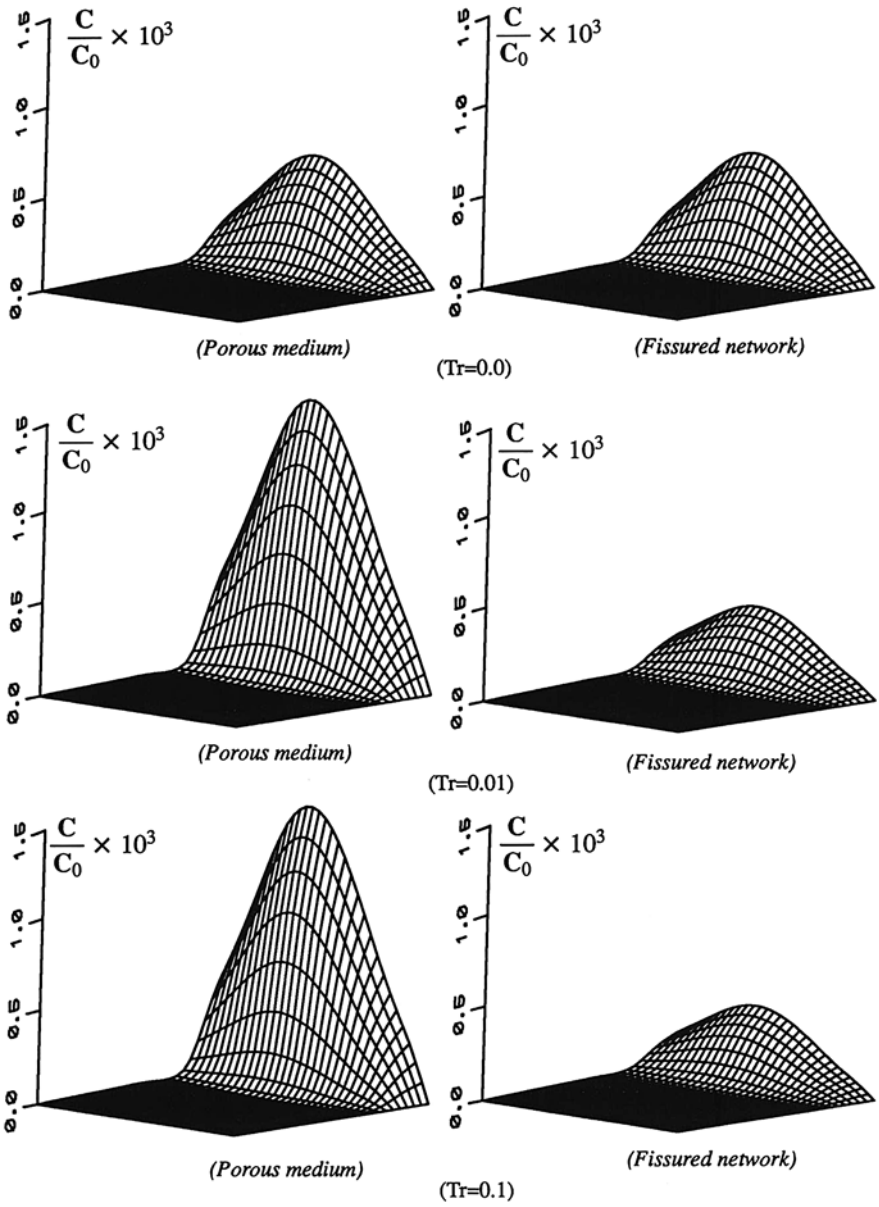

Fig. 8.11 Effects of leakages on dimensionless contaminant distributions in the fractured porous medium (t = 400 days)

the dimensionless concentration distribution of contaminant in the fractured porous medium. With an increase in the value of the transmissive coefficient, Tr, the maximum value of the dimensionless contaminant concentration increases in the porous block, but decreases in the fissured network. With $t = 100$ days taken as an example,

the maximum values of the dimensionless contaminant concentration in the case of no leakage (i.e. Tr = 0) between the two continua are 1.86 for both the porous block and the fissured network. However, the corresponding maximum values for Tr = 0.01(1/s) are 4.29 and 1.26 for the porous block and the fissured network, respectively. This indicates that a higher concentration may appear in the porous block because the porosity of the porous block is smaller than that of the fissured network in the computational model. Since advective pore-fluid flow is considered in the x direction only, both advection and dispersion take place in this direction, so that the contaminant transport speed in the x direction is much faster than that in the y direction.

With the increase of time, the maximum values of the dimensionless contaminant concentration in both the porous block and the fissured network decrease because the contaminant spreads over a broad area due to the development of solute advection and dispersion in the fractured porous medium. For instance, when Tr = 0.01(1/s), the maximum values of the dimensionless contaminant concentration are 4.29 and 1.26 at $t = 100$ days for the porous block and the fissured network, respectively, while they are 1.41 and 0.35 at $t = 400$ days for the porous block and the fissured network. The numerical results also indicate that the proposed coupled model of upwind finite elements and transient infinite elements reflects the mass conservation law very well during contaminant transport in the fractured porous medium. Since the contaminant has reached the right boundary of the upwind finite elements (at $x = 100$ m) in the x direction but only reached about one-third of the near field (at $y = 30$ m) in the y direction when $t = 400$ days, it can be concluded that pore-fluid flow advection plays an important role in the contaminant transport processes in fractured porous media of infinite domains. Although the transmissive coefficient between the porous block and the fissured network has a significant influence on the contaminant concentration distribution in the fractured porous medium, it has little effect on the contaminant transport speed in the coupled computational model of upwind finite elements and transient infinite elements.

Figures 8.12 and 8.13 show the dimensionless contaminant concentration versus time at six observation points in the computational model of the fractured porous medium. In these figures, the unit of time is day. Similarly, the results shown in the left columns are obtained for the porous continuum, while the results shown in the right columns are obtained for the fissured continuum. These results clearly indicate that the contaminant arrives at different observation points with different times. For example, the first arrival time of the contaminant at the observation point of $x = 20$ m and $y = 0$ m is about 20 days, while the corresponding arrival times at the other two observation points, namely ($x = 60$ m, $y = 0$ m) and ($x =$–20 m, $y = 0$ m), are about 100 and 35 days, respectively. Since the three observation points are located on the x axis and the contaminant source is located at the origin of the coordinate system when t = 0, both advection and dispersion take place at the three observation points in the fractured porous medium. Owing to the effect of a dispersion process, the contaminant arrives at the upstream observation point of $x = -20$ m and $y = 0$ m after it arrives at the downstream observation point of $x = 20$ m and $y = 0$ m. Through comparing the arrival time of the contaminant at an

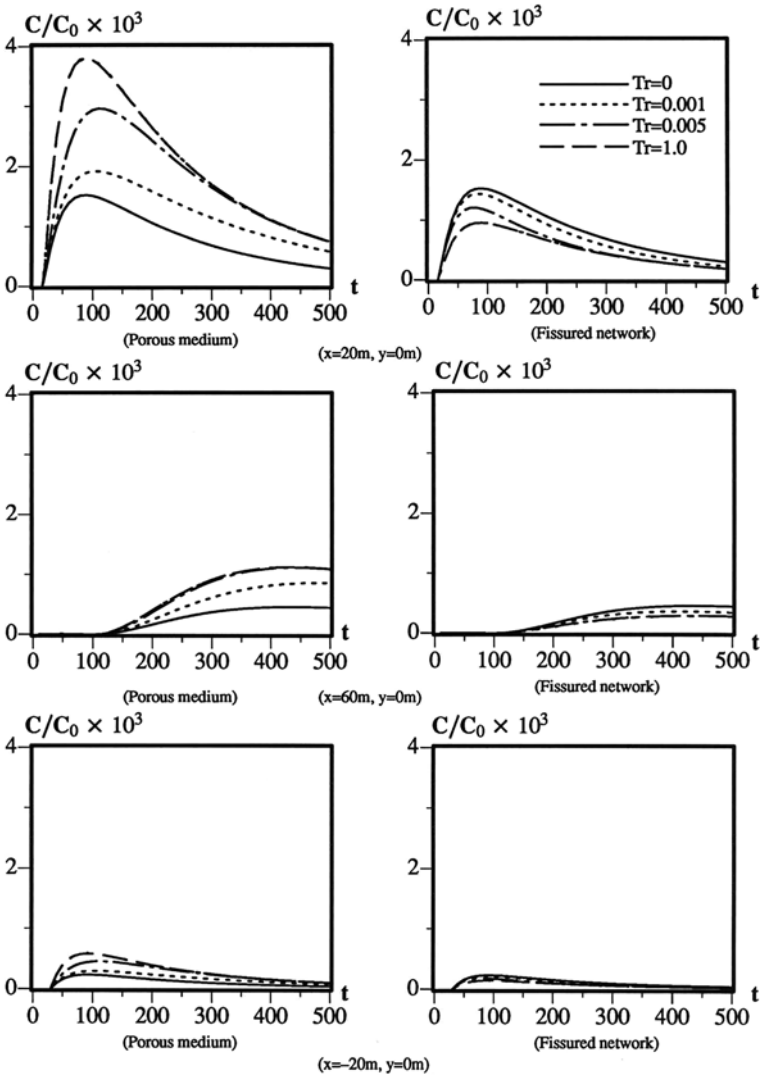

Fig. 8.12 Time-history distributions of dimensionless contaminant concentration due to different transmissive coefficients

observation point in the x axis with that at similar observation point, which is of the same distance from the origin of the coordinate system but is located in the y axis, it has been found that the contaminant travels much faster in the x direction than in the y direction. The first arrival time of the contaminant is 20 days for the observation point of $x = 20$ m and $y = 0$ m, while it is 200 days for the observation point of $x = 0$ m and $y = 20$ m. Since only dispersion takes place in the y direction, the first arrival time of the contaminant is identical for the three observation points shown

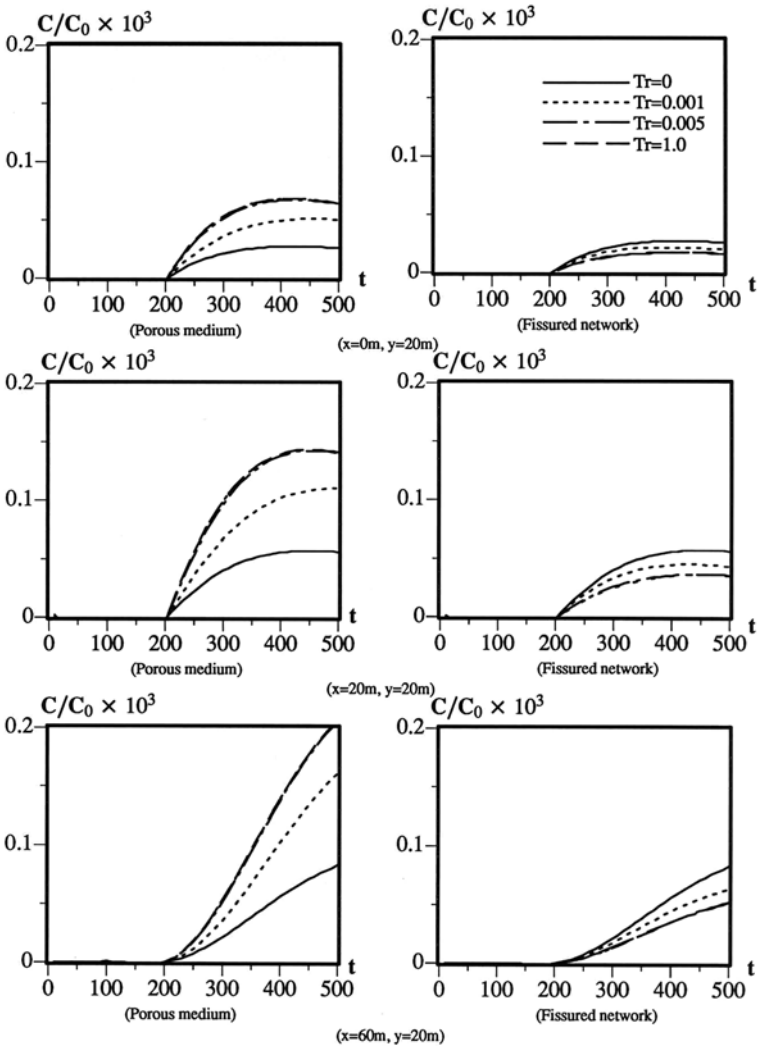

Fig. 8.13 Time-history distributions of dimensionless contaminant concentration due to different transmissive coefficients

in Fig. 8.13. These three observation points have the same y coordinates (i.e. $y =$ 20 m) but different x coordinates (i.e. $x = 0$, 20 and 60 m, respectively). Owing to the advection effect, the first arrival time of the contaminant is different for a pair of symmetric observation points at the x axis, as can be seen from the two observation points at $x = 20$ m and $x = –20$ m at the x axis of the coordinate system.

In terms of the leakage effect between the porous block and the fissured network on the contaminant transport process in the fractured porous medium, it has been recognized that when the transmissive coefficient, Tr, is within a range between 0 and 0.005 s^{-1}, any small change in its value can have a profound influ-

ence on the dimensionless contaminant concentration distribution in the fractured porous medium. However, when the transmissive coefficient becomes greater, an increase in its value has only some effects on the dimensionless contaminant concentration distribution in a limited adjacent region around the input contaminant source during the early period of time. This means that if the leakage effect between the porous block and the fissured network is weak, great caution should be taken for determining the value of the transmissive coefficient because it is very sensitive to the contaminant concentration distribution in both the near field and the far field of the system. On the other hand, if the leakage effect between the porous block and the fissured network is strong, any variation in the value of the transmissive coefficient has only a short-term effect on the contaminant concentration distribution in the near field of the system.

8.2.2 Effects of Medium Porosities on Contaminant Concentration Distributions in the Porous Block and Fissured Network

To investigate the effects of the porosities of the medium in both the porous block and the fissured network on contaminant transport processes in fractured porous media of infinite domains, the same fundamental problem as considered in Sect. 8.2.1 is simulated by the coupled computational model of upwind finite elements and transient infinite elements in this subsection. The following parameters are used in the coupled computational model. For the porous continuum, both the average linear velocities of pore-fluid flow and the dispersion coefficients in the x and y directions are exactly the same as those used in Sect. 8.2.1. For the fissured continuum, the average linear velocities of pore-fluid flow and the dispersion coefficients in the x and y directions are assumed to be the same as those used for the porous continuum. The transmissive coefficient between the porous and fissured continua is 0.01 (1/s). The porosity of the porous continuum (i.e. ϕ_1) is 0.05. Five different porosity ratios of the fissured continuum to the porous continuum, namely ϕ_2/ϕ_1=1, 2, 4, 6 and 10, are considered to investigate the effects of medium porosities on the contaminant concentration distribution in the fractured porous medium.

Figures 8.14 and 8.15 show the dimensionless concentration distribution of the contaminant in the near field of the first quadrant of the fractured porous medium at two different time instants. In these figures, n_2, is used to represent the porosity ratio of the fissured medium to the porous medium, ϕ_2/ϕ_1, so that $n_2 = \phi_2/\phi_1$ in this subsection. Clearly, the porosity ratio of the fissured medium to the porous medium has a significant influence on the dimensionless concentration distribution of the contaminant in the computational model of the fractured porous medium. The greater the porosity ratio of the fissured medium to the porous medium, the greater the dimensionless contaminant concentration in the near field of the porous medium is. Owing to the mass conservation of the contaminant, the greater the porosity ratio, the smaller the dimensionless contaminant concentration in the fissured medium is.

With an increase in the porosity ratio of the fissured medium to the porous medium, the maximum value of the dimensionless contaminant concentration

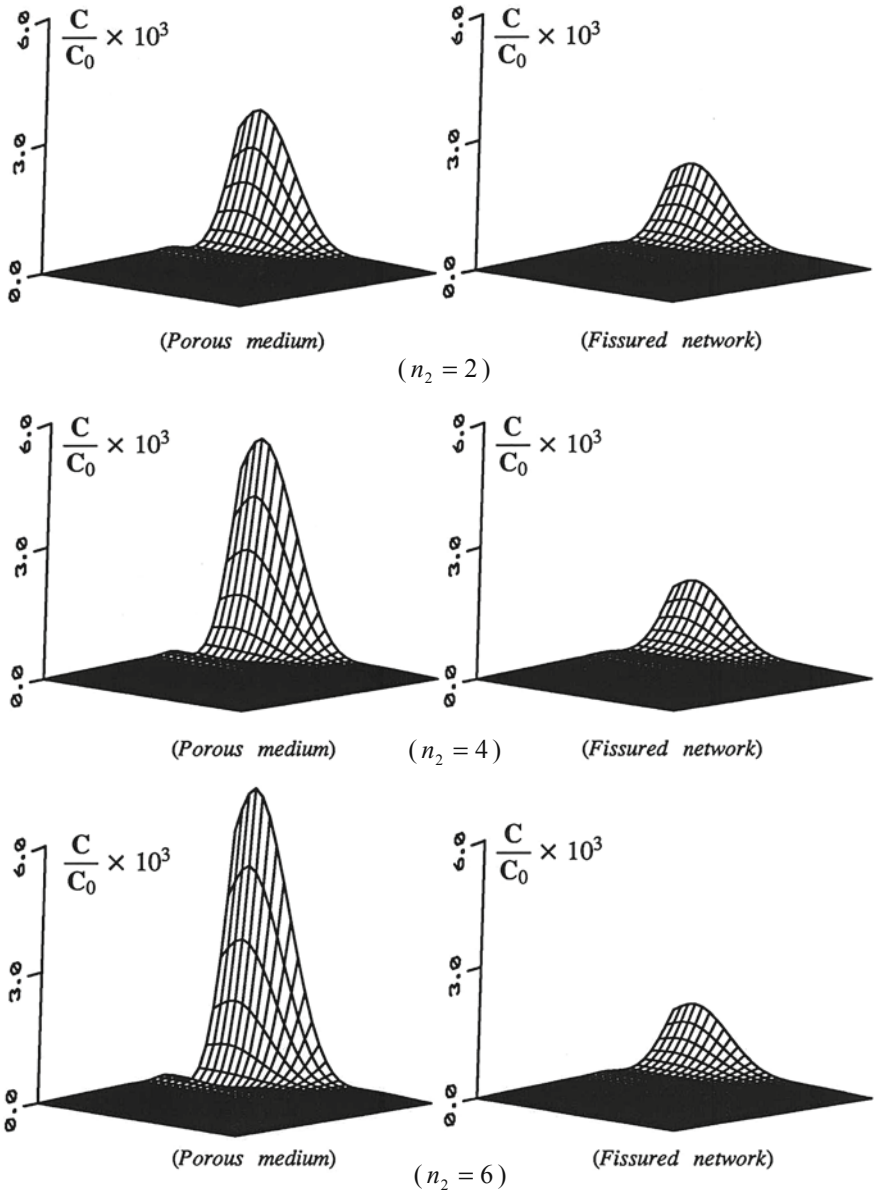

Fig. 8.14 Effects of porosity ratios on dimensionless contaminant distributions in the fractured porous medium (t = 100 days)

increases in the porous block but decreases in the fissured network. For example, the maximum values of the dimensionless contaminant concentration in the case of $n_2 = \phi_2/\phi_1$=2 are 1.575 and 0.795 for the porous block and the fissured network,

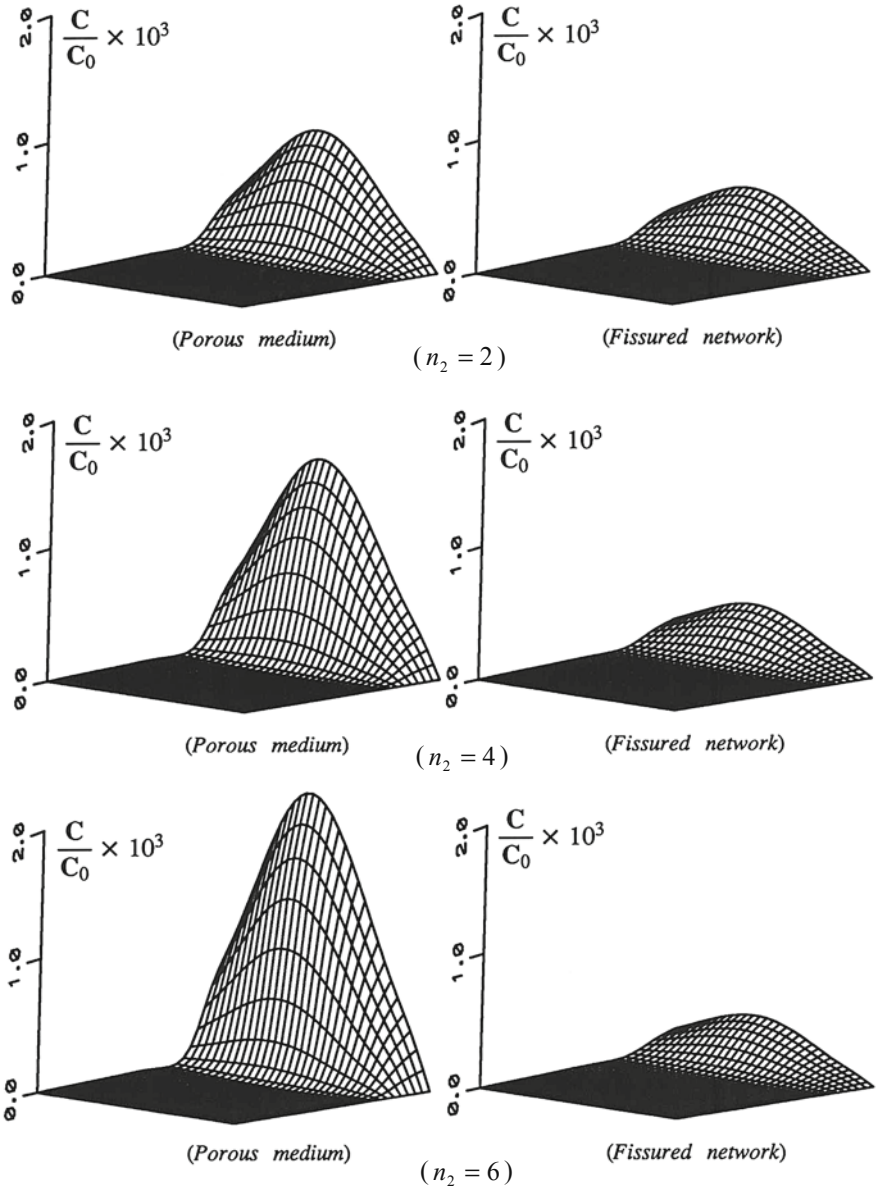

Fig. 8.15 Effects of porosity ratios on dimensionless contaminant distributions in the fractured porous medium (t = 400 days)

respectively, while the corresponding maximum values in the case of $n_2 = 6$ are 3.469 and 0.624, indicating that more contaminant may reside in the porous block when the porosity of the porous block is smaller than that of the fissured network. Since pore-fluid flow is considered in the x direction only, both advection and dispersion takes place in this direction, so that the contaminant transport speed in the x direction is faster than that in the y direction of the computational model. With the increase of time, the maximum value of the dimensionless contaminant concentration for both the porous medium and the fissured medium decreases as a result of the wide spread of the contaminant. Since the average linear velocity of the pore-fluid flow in the x direction is constant in the computational model, a change in the porosity ratio of the fissured medium to the porous medium has little effect on the contaminant transport speed in the computational model, even though it has a significant influence on the contaminant concentration distribution in the fractured porous medium.

Figures 8.16 and 8.17 show the dimensionless contaminant concentration versus time at several observation points of the computational model. Due to the consideration of a point contaminant source acting at the origin of the coordinate system at $t = 0$, the contaminant arrives at different observation points with different times, indicating that the contaminant concentration distribution is dependent on both space and time. Since the porosity ratio of the fissured medium to the porous medium and the transmissive coefficient between the porous medium and the fissured medium play similar roles in the contaminant transport process for the double porosity model of a fractured porous medium, the same conclusions as those obtained in Sect. 8.2.1 can be made on the first arrival time of the contaminant at a given observation point in the coupled computational model of upwind finite elements and transient infinite elements.

Regarding the effects of the porosity ratio of the fissured medium to the porous medium on the contaminant concentration distribution in the fractured porous medium, the related numerical results (in Figs. 8.16 and 8.17) indicate that within the parameter range studied, a slight change in the value of the porosity ratio can have a significant effect on both the short-term and the long-term contaminant concentration distributions in the fractured porous medium of infinite domain. For example, in the case of $x = 20$ m and $y = 0$ m, the dimensionless contaminant concentrations of the porous block at $t = 100$ days are 1.51, 2.16, 3.47, 4.77 and 7.38 for $n_2 = \phi_2/\phi_1 = 1$, 2, 4, 6 and 10, respectively, while the corresponding dimensionless contaminant concentrations at $t = 500$ days are 0.30, 0.45, 0.74, 1.04 and 1.63 for $n_2 = \phi_2/\phi_1 = 1$, 2, 4, 6 and 10. Although the dimensionless contaminant concentrations in both the porous block and the fissured network at each observation point vary as time goes on, their change rates are considerably different for different porosity ratios of the fissured medium to the porous medium in the fractured porous medium. This indicates that great caution should be taken for determining the value of the porosity ratio of the fissured network to the porous block because it can significantly affect the contaminant concentration distribution in both the near field and the far field of a fractured porous medium.

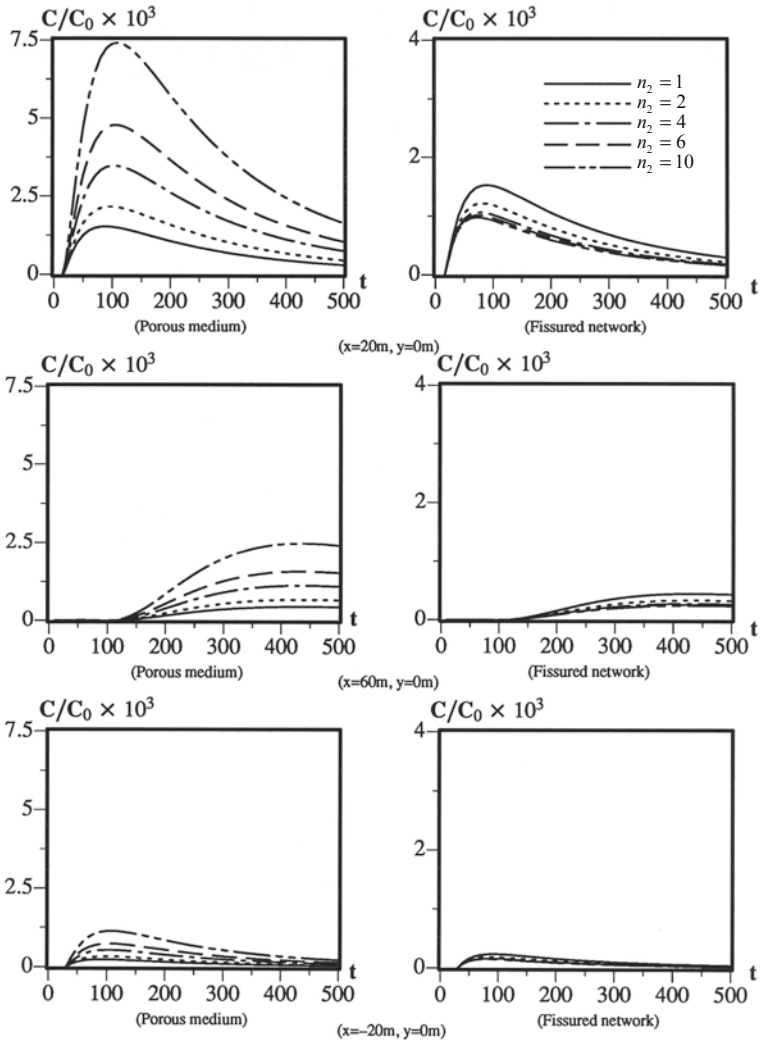

Fig. 8.16 Time-history distributions of dimensionless contaminant concentration due to different porosity ratios

8.2.3 Effects of Pore-Fluid Advection on Contaminant Concentration Distributions in the Porous Block and Fissured Network

The main purpose of this subsection is to investigate the effects of pore-fluid advection on contaminant concentration distributions in the porous block and fissured network of a fractured porous medium. For this purpose, a fundamental mass transport problem with an initial point contaminant source at the centre of a horizontal infinite plane consisting of a fractured porous medium is simulated using the coupled

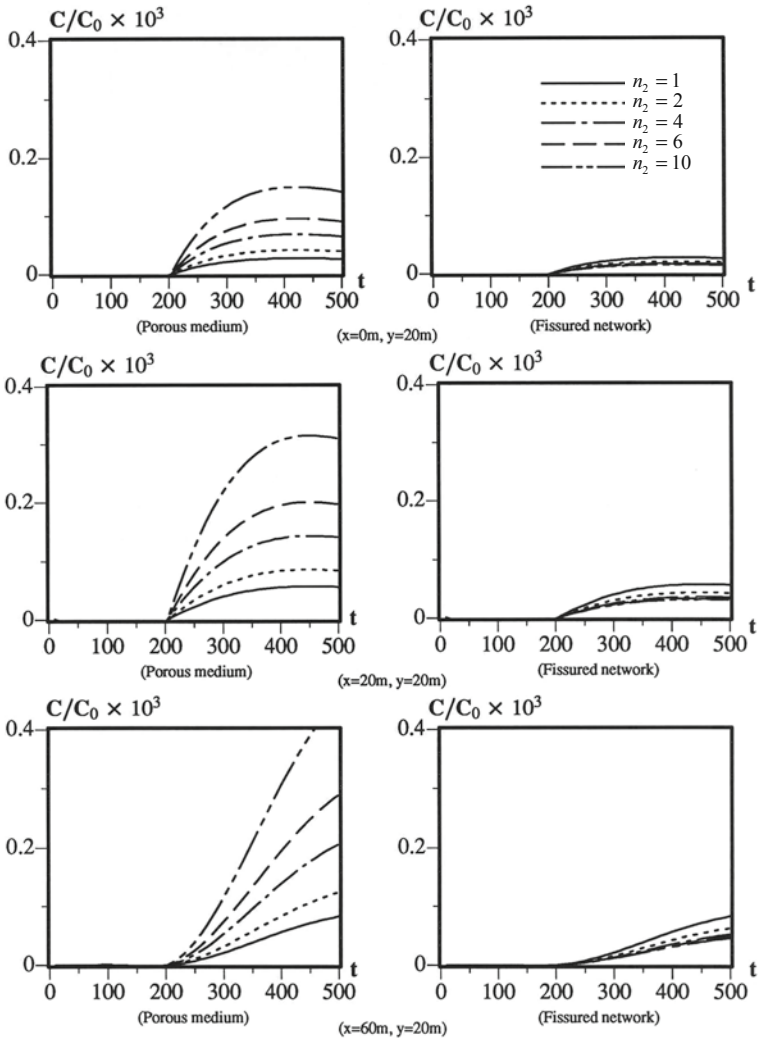

Fig. 8.17 Time-history distributions of dimensionless contaminant concentration due to different porosity ratios

computational method of upwind finite elements and transient infinite elements. With the porosity ratio, the dispersion coefficient and the transmissive coefficient kept constant, several different average linear velocities of pore-fluid flow are considered to examine the effects of pore-fluid advection on contaminant concentration distributions in the porous block and fissured network of a fractured porous medium.

The following parameters are used in the coupled computational model of the fractured porous medium. For the porous continuum, the dispersion coefficients are $1\,m^2d^{-1}$ and $0.1\,m^2d^{-1}$ in the x and y directions, respectively; the average linear velocity of the pore-fluid flow in the x direction (i.e. $\overline{V}_{1x}$) is 0.05 m d^{-1} when the

average linear velocity of the pore-fluid flow in the y direction (i.e. $\overline{V}_{1y}$) is equal to either 0 or 0.05 m d^{-1}. For the fissured continuum, the dispersion coefficients are 1 m^{2}d^{-1} and 0.1 m^{2}d^{-1} in the x and y directions, respectively; four different average linear velocities of the pore-fluid flow in the x direction, namely $\overline{V}_{2x}$=0.05, 0.1, 0.2 and 0.5 m d^{-1}, are considered in the case of $\overline{V}_{2y}$=0 m d^{-1}, while the average linear velocity of the pore-fluid flow in the x direction is 0.1 m d^{-1} in the case of $\overline{V}_{2y}$=0.1 m d^{-1}; the porosity ratio of the fissured continuum to the porous continuum is 4; the porosity of the continuum (i.e. ϕ_1) is 0.05; the transmissive coefficient between the porous block and the fissured network is 0.01 s^{-1}.

Figure 8.18 shows the effects of pore-fluid advection on the dimensionless concentration distribution of the contaminant in the near field of the first quadrant of the fractured porous medium at $t = 100$ days. In this figure, the numerical results associated with $\overline{V}_{2x}$= 0.05, 0.1 and 0.5 are obtained when the average linear velocities in the x and y directions are 0.05 m d^{-1} and 0 m d^{-1} in the porous continuum, but the average linear velocity in the y direction is 0 m d^{-1} in the fissured continuum. These results indicate that for three different values of the average linear velocity in the x direction within the fissured network, the distribution patterns of the dimensionless contaminant concentration are significantly different, implying that the average linear velocity of the pore-fluid flow has a remarkable influence on the dimensionless concentration distribution of the contaminant in the coupled computational model of the fractured porous medium.

Figures 8.19 and 8.20 show the dimensionless contaminant concentration distribution versus time at several observation points of the computational model. In these two figures, the numerical results marked by $\overline{V}_{2x}$= 0.05, 0.1, 0.2 and 0.5 are obtained when the average linear velocities in the x and the y directions are 0.05 m d^{-1} and 0 m d^{-1} in the porous continuum, but the average linear velocity in the y direction is 0 m d^{-1} in the fissured continuum. In contrast, the numerical results marked by $\overline{V}_{2x}$= 0.1 and $\overline{V}_{2y}$= 0.1 are obtained when the average linear velocities in both the x and the y directions are 0.05 m d^{-1} in the porous continuum. Obviously, the pore-fluid advection, which is represented by a different set of pore-fluid velocities, has a profound effect on the contaminant transport speed in the computational model of the fractured porous medium. The greater the average liner velocity of pore-fluid flow, the greater the contaminant transport speed in the fractured porous medium is.

For a given observation point, the average linear velocity of the pore-fluid flow affects not only the time-history distribution pattern, but also the maximum value of the dimensionless contaminant concentration in the fractured porous medium. With the three observation points (in Fig. 8.19) at the x axis taken as an example, the maximum value of the dimensionless contaminant concentration in the case of $\overline{V}_{1x} = \overline{V}_{1y}$=0.05 m d^{-1} and $\overline{V}_{2x} = \overline{V}_{2y}$=0.1 m d^{-1} is smaller than that in the other four cases. However, for the three observation points beyond the x axis (in Fig. 8.20), the maximum value of the dimensionless contaminant concentration in the case of $\overline{V}_{1x} = \overline{V}_{1y}$= 0.05 m d^{-1} and $\overline{V}_{2x} = \overline{V}_{2y}$=0.1 m d^{-1} is greater than that in the other four cases. This phenomenon is due to the fact that the contaminant can spread a broader area when advection takes place in both the x and y directions, compared

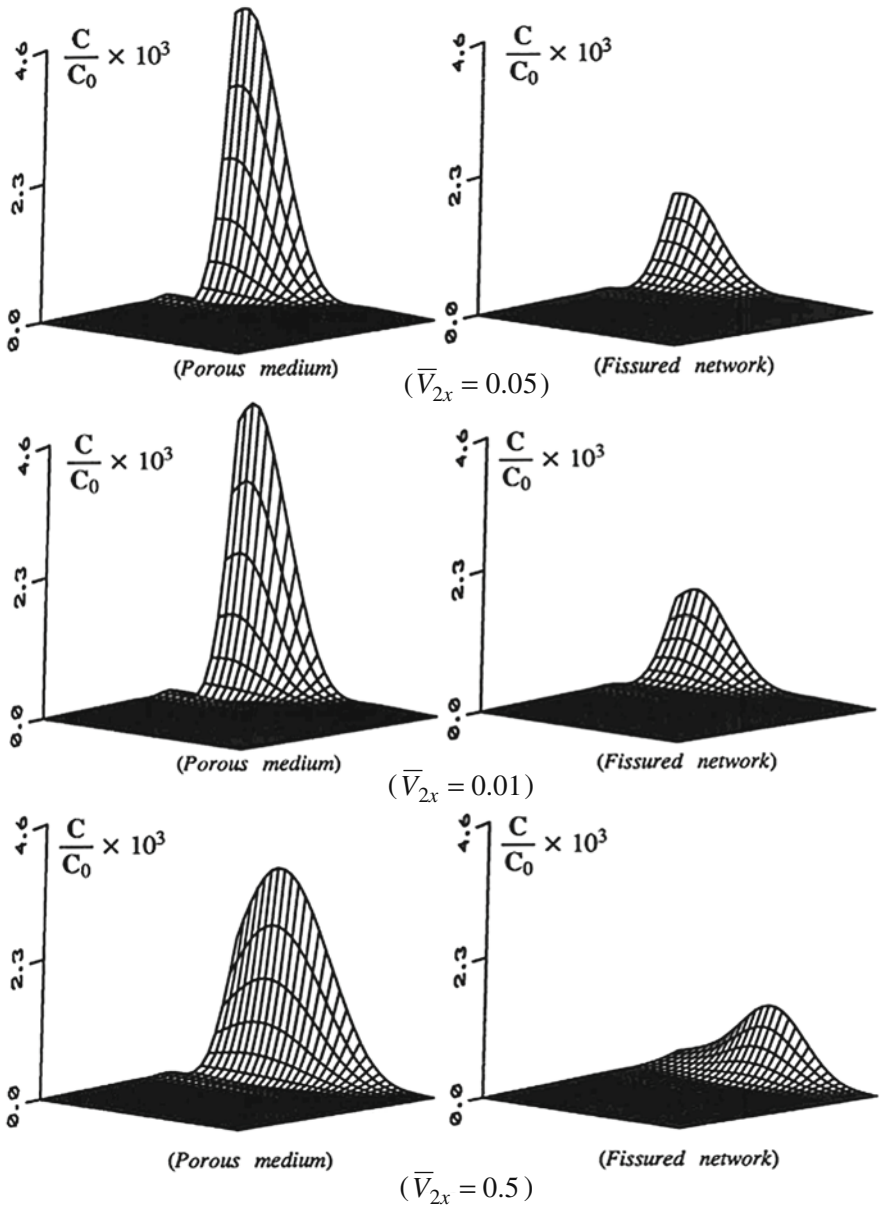

Fig. 8.18 Effects of pore-fluid advection on dimensionless contaminant distributions in the fractured porous medium (t = 100 days)

with when it takes place in the x direction only. Since the average linear velocity of pore-fluid flow affects both the contaminant transport speed and the maximum value of the contaminant concentration in a fractured porous medium, it should

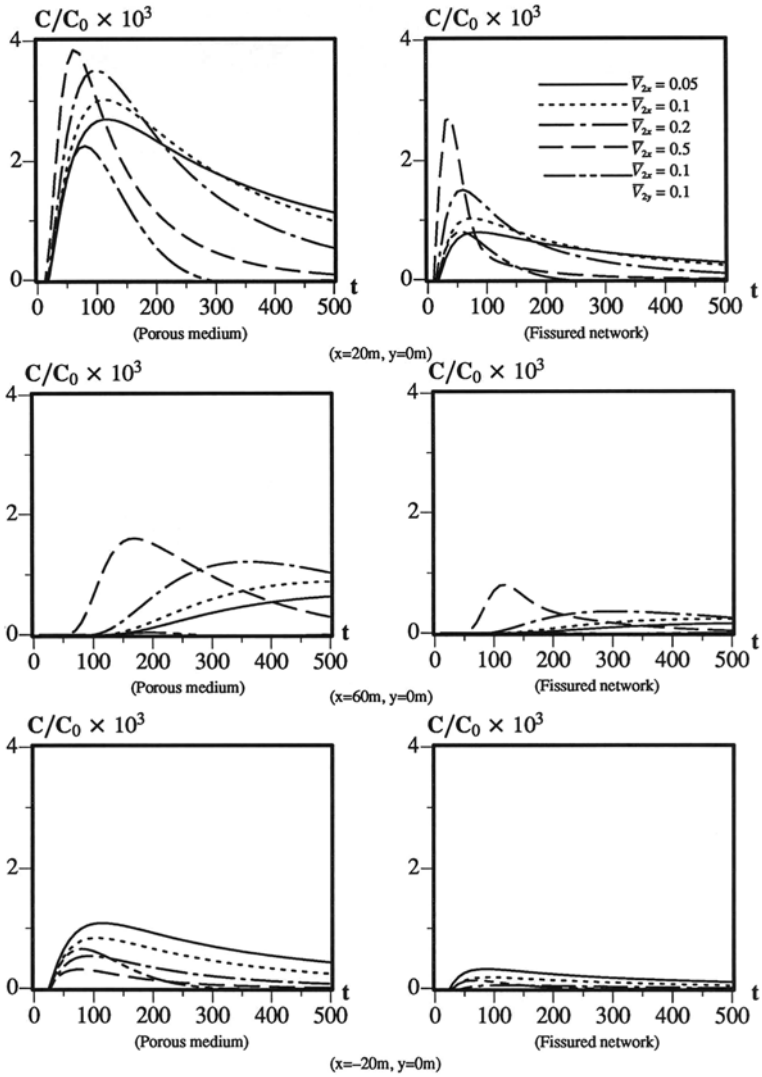

Fig. 8.19 Time-history distributions of dimensionless contaminant concentration due to different pore-fluid flow velocities

be determined carefully for the computational simulation of transient contaminant transport problems in fractured porous media of infinite domains.

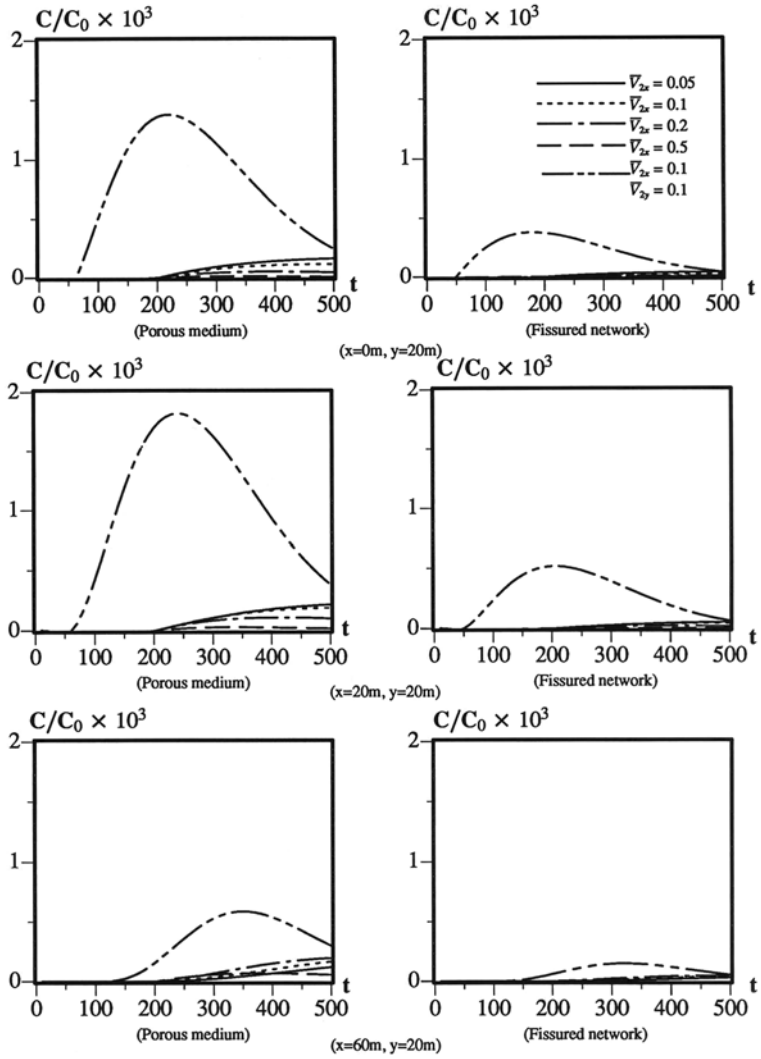

Fig. 8.20 Time-history distributions of dimensionless contaminant concentration due to different pore-fluid flow velocities

8.2.4 Effects of Solute Dispersion on Contaminant Concentration Distributions in the Porous Block and Fissured Network

To investigate the effects of solute dispersion in both the porous block and the fissured network on contaminant transport processes in fractured porous media of infinite domains, the same fundamental mass transport problem as that considered in the previous subsections is simulated by the coupled computational model of upwind

finite elements and transient infinite elements in this subsection. Through keeping the porosity ratio, the average linear velocity of pore-fluid flow and the transmissive coefficient constant, several different dispersion coefficients are considered to examine the effects of solute dispersion in both the porous block and the fissured network on contaminant transport processes in fractured porous media of infinite domains.

The following parameters are used in the coupled computational model. For the porous continuum, the average linear velocity of pore-fluid flow is 0.1 m d^{-1} in the x direction and zero in the y direction; the dispersion coefficient in the x direction (i.e. D_{1x}) is 1 m^2 d^{-1} when the dispersion coefficient in the y direction (i.e. D_{1y}) is equal to either 0.1 m^2 d^{-1} or 0.05 m^2 d^{-1}. For the fissured continuum, the average linear velocity of pore-fluid flow is 0.1 m d^{-1} in the x direction and zero in the y direction; four different dispersion coefficients in the x direction, namely D_{2x}= 0.2, 0.5, 0.7 and 1.0 $m^2 d^{-1}$, are considered when the dispersion coefficient in the y direction (i.e. D_{2y}) is equal to 0.1 m^2 d^{-1}; while only the dispersion coefficient of 0.2 m^2 d^{-1} in the x direction is considered when the dispersion coefficient in the y direction is equal to 0.2 m^2 d^{-1}; the porosity ratio of the fissured continuum to the porous continuum is 4; the porosity of the porous continuum (i.e. ϕ_1) is 0.05; the transmissive coefficient between the porous block and the fissured network is 0.01 s^{-1}.

Figure 8.21 shows the effects of solute dispersion on the dimensionless concentration distribution of the contaminant in the near field of the first quadrant of the fractured porous medium at $t = 100$ days. In this figure, the numerical results associated with D_{2x}= 0.2, 0.5 and 1.0 are obtained when the dispersion coefficient of the porous continuum are 1.0 and 0.1 m^2 d^{-1} in the x and y directions, respectively, while the dispersion coefficient of the fissured continuum (i.e. D_{2y}) is 0.1 m^2 d^{-1} in the y direction. These results indicate that for the three different dispersion coefficients of the fissured network in the x direction, the distribution patterns of the dimensionless contaminant concentration are significantly different, implying that the solute dispersion has a remarkable influence on the dimensionless concentration distribution of the contaminant in the coupled computational model of the fractured porous medium.

Figures 8.22 and 8.23 show the dimensionless contaminant concentration distribution versus time at several observation points of the computational model. In these two figures, the numerical results marked with D_{2x}= 0.2, 0.5, 0.7 and 1.0 are obtained when the dispersion coefficients of the porous continuum are 1.0 and 0.1 m^2 d^{-1} in the x and y directions, while the dispersion coefficients of the fissured continuum is 0.1 m^2 d^{-1} in the y direction. On the other hand, the numerical results marked with D_{2x}= 0.2 and D_{2y}= 0.2 are obtained when the dispersion coefficients of the porous continuum are equal to 1.0 m^2 d^{-1} in both the x and y directions. Clearly, the solute dispersion, which is represented by a different set of dispersion coefficients in this study, has a profound effect on the contaminant transport speed in the computational model of the fractured porous medium. The greater the dispersion coefficient, the greater the contaminant transport speed in the fractured porous medium is.

Similarly, for a given observation point, the solute advection affects not only the time-history distribution pattern, but also the maximum value of the dimensionless contaminant concentration in the fractured porous medium. For the three observa-

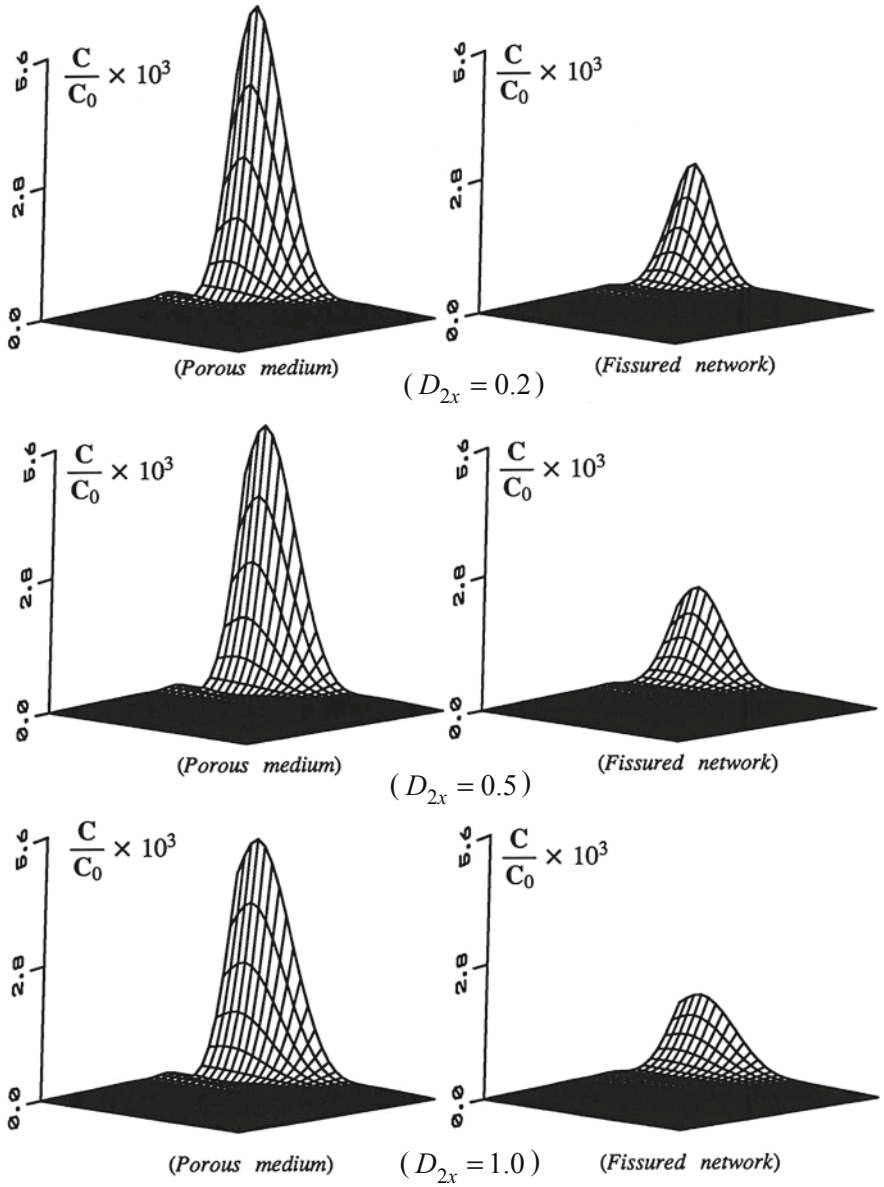

Fig. 8.21 Effects of solute dispersion on dimensionless contaminant distributions in the fractured porous medium (t = 100 days)

tion points (in Fig. 8.22) at the x axis, the maximum value of the dimensionless contaminant concentration in the case of $D_{1x} = D_{1y}$=1.0 m^2 d^{-1} and $D_{2x} = D_{2y}$= 0.2 m^2 d^{-1} is smaller than that in the other four cases. However, for the three observation points beyond the x axis (in Fig. 8.23), the maximum value of the dimen-

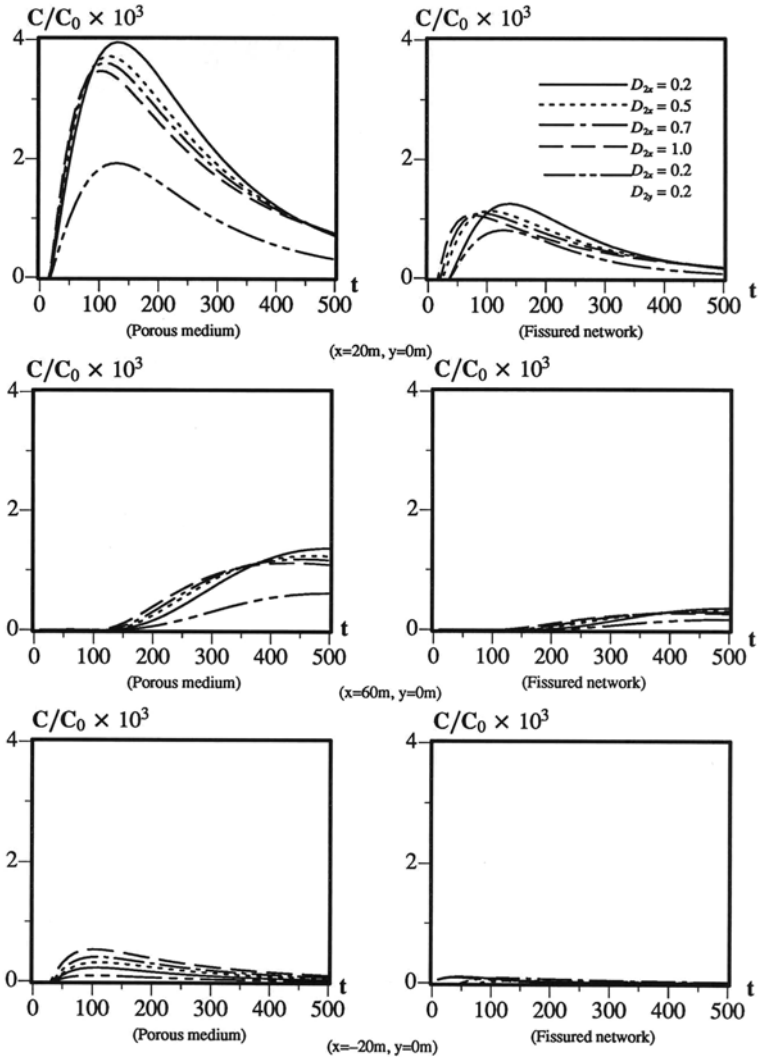

Fig. 8.22 Time-history distributions of dimensionless contaminant concentration due to different dispersion coefficients

sionless contaminant concentration in the case of $D_{1x} = D_{1y}$=1.0 m^2 d^{-1} and $D_{2x} = D_{2y}$=0.2 m^2 d^{-1} is greater than that in the other four cases. Since dispersion coefficients can affect both the contaminant transport speed and the maximum value of the contaminant concentration in a fractured porous medium, they should be determined carefully in the coupled computational model of upwind finite elements and transient infinite elements for simulating transient contaminant transport problems in fractured porous media of infinite domains.

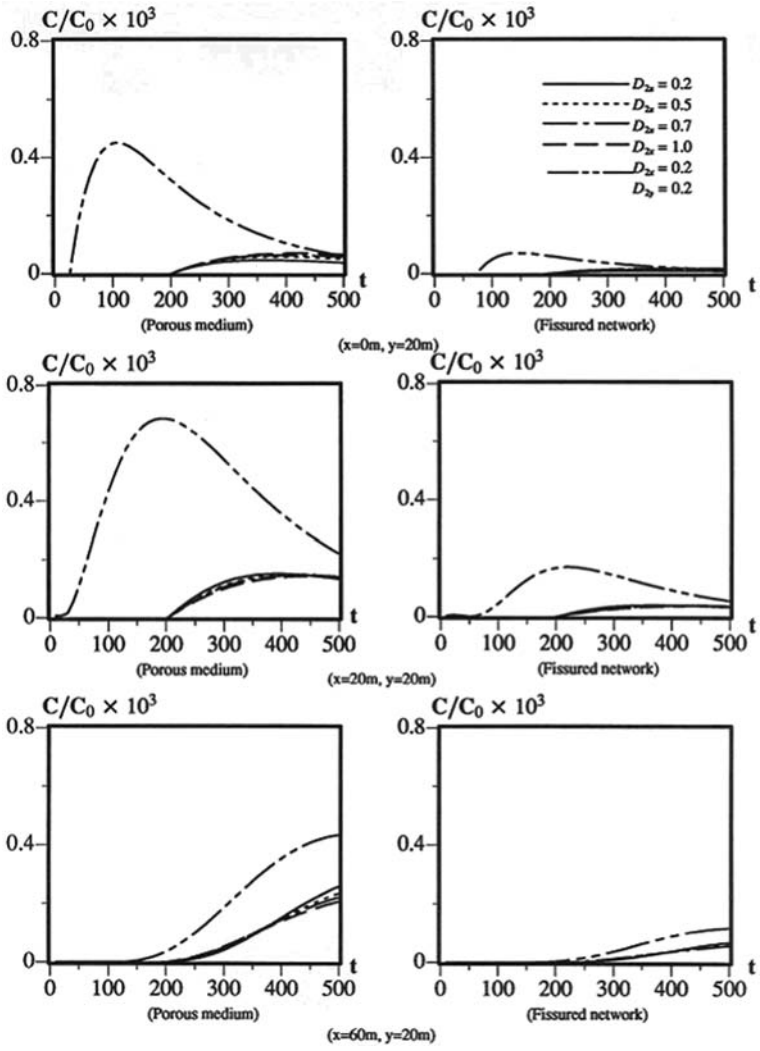

Fig. 8.23 Time-history distributions of dimensionless contaminant concentration due to different dispersion coefficients

In summary, the leakage between the porous block and the fissured network has a significant influence on the distributions of the contaminant concentration in fractured porous media. Generally, the maximum value of the contamination concentration increases in the porous block, but it decreases in the fissured network as a result of the leakage between the porous block and the fissured network. This indicates that more contaminant resides in the porous block. With the increase of time, the maximum values of the contaminant concentration in both the porous block and the fissured network decrease as the contaminant spreads over a broad area.

The transmissive coefficient between the porous block and the fissured network has little effect on the transport speed of the contaminant, even though it has a significant influence on the values of the contaminant concentration in a fractured porous medium.

Considering the effect of the porosities of the fractured porous medium, a larger porosity of the fissured network results in a greater value of the contaminant concentration in the near field of the porous block, whereas it results in a smaller value in the near field of the fissured network. With an increase in the porosity of the fissured network, the maximum value of the contaminant concentration increases in the porous block but decreases in the fissured network.

The average linear velocity (representing the advection) of pore-fluid flow has a significant influence on both the concentration distribution pattern and the transport speed of the contaminant in the fractured porous medium. The larger the average linear velocity of the pore-fluid flow is, the greater will be the transport speed of the contaminant in both the porous block and the fissured network. The same conclusion can be made when the effect of the dispersion is considered in the fractured porous medium.